Chapter 4

EGFR and glycan receptor targeted chitosan nanoparticles of gemcitabine

4 EGFR and glycan receptor targeted chitosan nanoparticles for enhanced active cellular internalization of gemcitabine in lung cancer therapy.

4.1 Objective

The objective of this study was to optimize chimeric monoclonal antibody cetuximab (Cxmab) conjugated CSN nanoparticles and develop dual targeted (EGFR and glycan) chitosan nanoparticles loaded with gemcitabine for lung cancer treatment. The prepared nanoparticles characterized in terms of their physiochemical characterization, *in vitro* release mechanism, *in vitro* cellular uptake, cytotoxicity, effect on metastasis, analysis of apoptosis on A549 cells and *in vivo* (pharmacokinetics) in rats and *in vivo* therapeutic efficacy in B[a]P induced lung cancer in swiss albino mice. Results of gemcitabine loaded dual receptor targeted chitosan NPs were compared to single receptor targeted, non-targeted and marketed gemcitabine (gemzer) injectable formulation.

4.2 Plan of study

1) Optimization of gemcitabine loaded chimeric mAb conjugated chitosan nanoparticles
2) Preparation of gemcitabine loaded targeted and non-targeted chitosan nanoparticles
3) Characterization of nanoformulations
   i. Measurement of particle size, polydispersity index and zeta potential (surface charge)
   ii. HPLC method for determination of gemcitabine
   iii. Determination of entrapment Efficiency (%EE)
   iv. Morphological evaluation by transmission electron microscopy (TEM), scanning electron microscopy (SEM) and atomic force microscopy (AFM) analysis
   v. X-ray diffraction (XRD), Differential scanning calorimetry (DSC) analysis, Fourier transform infrared (FTIR) spectroscopy analyse the physical state of gemcitabine in nanoparticles
   vi. Surface chemistry by X-ray photoelectron spectroscopy (XPS) analysis
   vii. Estimation of concentration of Neu5Ac conjugated on the surface of nanoparticles
   viii. Estimation of cetuximab concentration conjugated on the surface of nanoparticles

4) *In vitro* studies

i. Evaluation of *in vitro* drug release study of gemcitabine from nanoparticles

ii. Analysis of cellular uptake in A-549 lung cancer cell line

iii. Cytotoxicity study by MTT in A-549 lung cancer cell line

iv. Effect on Metastasis (Wound Healing Assay) on A-549 lung cancer cell line

v. Annexin-V/PI apoptosis assay on A-549 lung cancer cell line

5) *In vivo* studies

i. *In vivo* pharmacokinetic evaluation of gemcitabine

ii. *In-vivo* biochemical investigation

iii. *In vivo* therapeutic efficacy in B[a]P induced lung cancer in swiss albino mice

4.3 Material

Gemcitabine hydrochloride was obtained as a gift sample from Neon Laboratories Pvt. Ltd., Mumbai India. Chitosan, degree of deacetylation min. 90%, N-acetylneuraminic acid (NANA, Sialic acid), Bradford and Ehrlich reagent were purchased from Sisco Research Laboratories (SRL)-India. The dialysis membrane-70 (MW 14000 Dalton) was obtained from HiMedia Laboratories Pvt. Ltd.-Mumbai, India. Acetic acid, sodium hydroxide (NaOH) pellets, HPLC quality water, acetonitrile, Dimethyl sulfoxide, ethanol and methanol were bought from Merk Life Science-India. Sodium TPP, coumarin-6, penicillin, streptomycin and cetuximab, Benzo-(a)-Pyrene, urethane were purchased from Sigma-Aldrich. Clinical formulation GEMCIT utilized as drug control, was provided by *Getwell* Oncology Pvt. Ltd., Gurugram, India. The A-549 cell lines (human lung adenocarcinoma) were supplied by the National Centre for Cell Science (NCCS), Pune-India. Trypsin-EDTA, Dulbecco's modified Eagle's medium (DMEM), Fetal bovine serum (FBS), 3-(4,5-dimethyl thiazolyl-2-yl)-2,5-diphenyltetrazolium bromide (MTT) were obtained from Thermo Fisher Scientific-India.

4.4 Methods

4.4.1 Optimization of chimeric mAb conjugated chitosan nanoparticles

One factor three-level one response Box-Behnken design approach shown in **Table 4.1** was used to determine the optimum amount of cetuximab that can be efficiently conjugated to the chitosan nanoparticles. The already optimized chitosan nanoparticles **(section 3.4.2)** were used for the experimental design. The Cxmab was conjugated by incubating required quantities of Cxmab to GMC-CSN-NPs overnight via electrostatic interaction.

Bradford assay was used to determine the amount of Cxmab upon conjugation on the surface of chitosan nanoparticles [247]. For this 50 µL of GMC-CSN-Cxmab-NPs, 50 µL phosphate buffer saline (PBS) pH 7.4 and 250 µL of Bradford reagent were added to 96-well plate and incubated for 5 min in darkness. PBS pH 7.4 was utilised as a negative control. Then UV-Visible absorbance was recorded on a multi-mode microplate reader at 590 nm (Molecular devices, USA). The Content of Cxmab was measured by using the standard curve of bovine serum albumin [248] using following equation:

$$Content\ of\ Cxmab\ conjugation = \frac{Content\ of\ Cxmab\ in\ NPs - Content\ of\ Cxmab\ in\ blank\ (PBS)}{Content\ of\ Cxmab\ in\ standard\ solution} * 100$$

Table 4.1 Experimental design with levels of variables to optimize the amount of monoclonal antibody (cetuximab) to be conjugated to chitosan nanoparticles

Factors/Responses		Levels		
		Low level (-1)	**Medium level (0)**	**High level (+1)**
Independent Variables (Factors)	Cetuximab (mg)	1	1.5	2
Dependent Variables (Responses)	Conjugation of cetuximab (%)		Maximum	

4.4.2 Preparation of gemcitabine loaded targeted and non-targeted chitosan nanoparticles

Gemcitabine encapsulated targeted and non-targeted nanoformulations shown in **Figure 4.1 A, B** were prepared by previously described ionic gelation process with slight changes [249]. Appropriate amounts of CSN and CSN-Neu5Ac, as listed in **Table 4.2**, were added to the 0.2% v/v aqueous acetic acid solution. The pH of the aforementioned mixture was adjusted to 5.5 with aqueous NaOH solution. After 30 min of stirring 10 mg of gemcitabine was dissolved in 1 mL of water and finally added to chitosan solution. The above solution was kept for stirring for 3 h at 800-1000 rpm. In order to cross-link chitosan solution, 8 mL of a sodium tripolyphosphate (Na-TPP) solution diluted to 0.5 mg/mL with water, was added gently drop wise, and stirred for 2 hr. To achieve surface conjugation of cetuximab (Cxmab) through electrostatic interaction on CSN-NPs, briefly, 0.4 mL (2mg) of Erbitux (Cxmab 5 mg/mL) was added to each of 20 mL of prepared GMC-CSN-NPs and GMC-CSN-Neu5Ac-NPs and incubated overnight to form GMC-CSN-Cxmab-NPs and GMC-CSN-Neu5Ac-Cxmab-NPs respectively. Further, centrifugation at 12000 rpm for 30 min was performed to purify the nanoparticles. Supernatant was discarded and the NPs residue was re-suspended in water followed by freeze drying to get dry powder for further use or analysis.

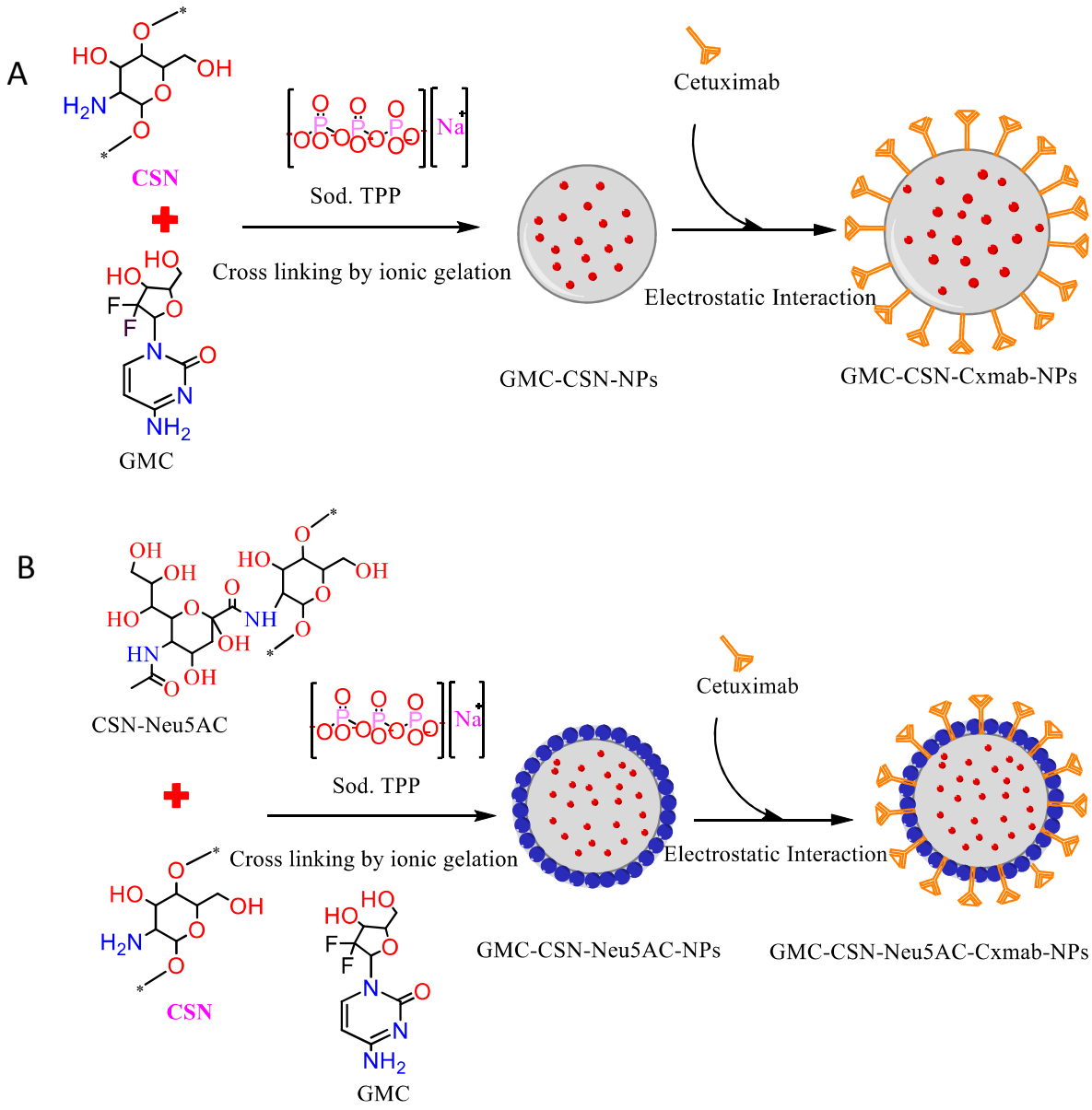

Figure 4.1 Formulation of gemcitabine loaded A. Chitosan nanoparticles (GMC-CSN-NPs), cetuximab conjugated chitosan nanoparticles (GMC-CSN-Cxmab-NPs) B. Neu5Ac conjugated chitosan nanoparticles (GMC-CSN-Neu5Ac-NPs), Neu5Ac and cetuximab conjugated chitosan nanoparticles (GMC-CSN-Neu5Ac-Cxmab-NPs).

Table 4.2 Preparation of gemcitabine loaded non-targeted and targeted chitosan nanoparticles.

Nanoformulations	CSN-Neu5Ac (mg)	CSN (mg)	Cxmab (mg)	GMC (mg)	Na-TPP (mg)
GMC-CSN-NPs	0	20	0	10	4
GMC-CSN-Neu5Ac-NPs	10	10	0	10	4
GMC-CSN-Cxmab-NPs	0	20	2	10	4
GMC-CSN-Neu5Ac-Cxmab-	10	10	2	10	4

NPs

Note: GMC-CSN-NPs: GMC loaded chitosan NPs, GMC-CSN-Neu5Ac-NPs: GMC loaded Neu5Ac conjugated chitosan NPs, GMC-CSN-Cxmab-NPs: GMC loaded Cetuximab conjugated chitosan NPs, GMC-CSN-Neu5Ac-Cxmab-NPs: GMC loaded Cetuximab and Neu5Ac conjugated chitosan NPs.

4.4.3 Characterization of nanoformulations

4.4.3.1 Measurement of particle size, polydispersity index and zeta potential (surface charge)

Particle mean diameter, polydispersity index (PDI) and surface charge of the formulations was analysed by dynamic light scattering technique (Malvern Zetasizer Nanoseries) at 25 ◦C [250]. For the measurements of particle size and PDI, 100 µL of aqueous dispersion of freeze dried CSN-NPs (1 mg/mL) were diluted ten times (1:10) with deionized water and then bath sonicated to retain and reduce the aggregation of the particles in suspension. Approximately 1 mL of NPs solution was filled in disposable polystyrene cells and then analysed. The particle size and PDI of the nanoformulations was obtained by calculating the average of 12 measurements at a fixed angle [251].

For zeta potential measurement aqueous dispersion of freeze dried CSN-NPs (1 mg/mL) was vortexed for 2 min at normal temperature and then transferred to a plain folded zeta cell (DTS1060C, Malvern Instruments) by 1 mL disposable syringe through one of the ports on the zeta cell (maximum fill volume in zeta cell is 0.75 mL). Air bubbles were removed from the cell and both ends of cell were capped to confirm equal sample levels on both sides of the zeta cell before being inserted cell into the instrument. All measurements were performed in triplicate to establish measurement repeatability [217].

4.4.3.2 HPLC method for determination of gemcitabine

The chromatographic separation of gemcitabine were done on C18 column (shodex C18, 250x4.6mm, 5um) operated at 30°C using reversed-phase high-performance liquid chromatography (RP-HPLC) Agilent system using mobile phase composition of methanol: water in 20:80 ratio, at a constant flow rate of 1 millilitre per minute (mL/min). The analysis was performed at a wavelength of 272 nm on PDA detector.

4.4.3.3 Determination of entrapment efficiency (%EE)

The GMC entrapped in nanoparticles was analysed by ultracentrifugation method. In order to separate the free GMC fraction from the nanoformulations, briefly, 2mL nanoparticulate suspension was centrifuged at 12,000 rpm for 30 min by cooling centrifuge (REMI *ELEKTROTECHNIK LTD.,* C-24 PLUS, ZDFU-16439) [252]. The supernatant was then separated and the free drug was estimated by HPLC. Resultant supernatant was filtered through 0.22 μm size syringe filter. Approximately 10 μL of filtered supernatant was diluted 100 times with HPLC grade Milli-Q water. After filtration and dilution, 500 microliter (μL) diluted sample was added to HPLC vials and placed in HPLC tray for analysis. 20 μL sample from each vial was automatically injected *via* the auto sampler. The analysis was performed using methanol: water mixture (20:80) as mobile phase, at a flow rate of 1 mL/min and temperature 30°C with the peak detection wavelength of 272 nm on a PDA detector. The total amount of GMC in targeted and non-targeted CSN-NPs was calculated from the peak area aligned with the standard curve. The following method was used to calculate the percentage of Entrapment:

$$\%EE = \frac{Total\ amount\ of\ GMC - Amount\ of\ free\ GMC}{Total\ amount\ of\ GMC} * 100$$

4.4.3.4 Analysis of surface morphological characteristics of nanoparticles

4.4.3.4.1 Transmission electron microscopy (TEM) analysis

Analysis using transmission electron microscopy (TEM) was done to determine the formulation's shape and particle size [253]. The ultra-pure water was used to dilute 100 μL of each of nanoparticle formulation ten times followed by sonication on bath sonicator for 5 min. The nanoparticle solution was applied on a copper TEM grid, after which the sample was dried at room temperature, which was then exposed to TEM analysis.

4.4.3.4.2 Scanning electron microscopy (SEM) analysis

The morphological characteristics (aggregation and shape) of CSN-NPs were examined by scanning electron microscope (SEM) (FEI-USA (S.E.A.) PTE, LTD) [254]. All nanoparticle formulations (100 μL each) were diluted ten times with milli-Q water followed by bath sonication. A single drop of

diluted nanoparticle solution was dropped on a glass slide, which was then dried at 40–45 °C overnight in a hot air oven before analysis and then analysed under SEM.

4.4.3.4.3 Atomic force microscopy (AFM) analysis

Atomic force microscopy (AFM) examination was carried out to see the surface morphology of the nanoformulations (NT-MDT Service & Logistics Ltd. Moscow, Russia) [255]. In brief, the nanoparticle solution was diluted (ten times) with milli-Q water then bath sonicated for 10 min. The specimens were made by depositing a droplet of NPs on a glass coverslip and allowed to immobilise for 1-2 min, then vacuum dried for 24 h to produce a thin film. The surface morphology of NPs was then examined by putting them on an AFM scanner and imaging them in tapping mode at scanning rate of 0.5 Hz. SOLVER NEXT software was used for dimensional analysis of 2D and 3D images of NPs.

4.4.3.5 Solid state characterization of nanoparticles

4.4.3.5.1 X-ray diffraction (XRD) analysis

To study the crystalline/amorphous nature of the NPs and confirm their physical condition within the NPs, XRD analysis of lyophilized samples was performed. The Rigaku portable X-ray diffractometer was used to generate the XRD spectrum of non-targeted, targeted formulations and pure drug (Rigaku, Japan) [249]. The XRD patterns were produced using Cu-K radiation filtered through Ni, at a voltage of 45 kV, in the scanning range of 2θ of 20°-80°, using a current of 40 mA distributed in the sample's crystalline areas, and monitored using a vertical goniometer.

4.4.3.5.2 Differential scanning calorimetry (DSC) analysis

The physical state of GMC encapsulated in the targeted and non-targeted CSN-NPs and the pure GMC was examined by DSC (DSC-60 plus SHIMADZU) under liquid nitrogen at flow rate of 100 mL/min. 5 mg of each sample was heated from 20°C to 300°C increasing at a speed of 10°C/min.

4.4.3.5.3 Fourier transform infrared (FTIR) spectroscopy

Entrapment of GMC into CSN-NPs was also checked qualitatively by FTIR spectrometry. FTIR spectra for free GMC, GMC-CSN-NPs, GMC-CSN-Neu5Ac-NPs, GMC-CSN-Cxmab-NPs and

GMC-CSN-Neu5Ac-Cxmab-NPs were obtained from FTIR spectrophotometer (THERMO Electron Scientific) for characterizing the chemical integrity of GMC inside CSN-NPs. Briefly, the 1 mg of each sample was pressed with KBr to make a pellet by hydraulic press. FTIR spectra were scanned over spectral range of 4000-400cm^{-1} with a resolution of 4 cm^{-1} [256].

4.4.3.6 Evaluation of surface chemistry of nanoparticles

X-ray photoelectron spectroscopy (XPS) analysis (Thermo Fisher Scientific, K-Alpha) was used to examine the surface chemistry of nanoformulations at 100-800 eV. A drop of nanoparticle suspension was used to prepare the samples for analysis, which was then dried overnight in a vacuum dryer. XPS provides information regarding interaction between the surfaces of chitosan nanoparticles coated with Neu5Ac and Cxmab. Particularly, XPS exposes the atomic makeup of the surface of the nanoparticles [257].

4.4.3.7 Estimation of amount of 5-N-acetyl-neuraminic acid in CSN-Neu5Ac conjugate and nanoparticles

The concentration of Neu5Ac in CSN-Neu5Ac conjugate, GMC-CSN-Neu5Ac-NPs and GMC-CSN-Neu5Ac-Cxmab-NPs was quantified by earlier defined procedure with minor changes [258]. Briefly, 200 µL of CSN-Neu5Ac conjugate solution in milli-Q water was incubated with 1500 µL of 5% perchloric acid (HClO4) for 5-10 min at 100 °C. After cooling the solution, it was centrifuged at 2500-3000 rpm for 5 min. After that 1 mL of supernatant was mixed with 200 µL of Ehrlich's reagent and again heated at 100°C for 15-20 min. The solution was subjected to cooling and then 1 mL milli-Q water was added into it. Subsequently, the absorbance of the colour produced in the solution was determined at 525 nm using UV-Vis spectrophotometer (Synergy H1 Microplate Reader). A standard calibration curve was plotted from absorbance of known concentrations of Neu5Ac (N-acetylneuraminic acid) solution in milli-Q water by the above defined method that was used to quantify the extent of Neu5Ac [258].

$$Extent\ of\ Neu5Ac\ (\%) = \frac{Total\ Neu5Ac\ content\ in\ NPs}{Neu5Ac\ content\ determined\ in\ CSN\_Neu5Ac} * 100$$

4.4.3.8 Estimation of cetuximab concentration conjugated on surface of nanoparticles

Bradford assay was used to determine the content of Cxmab upon conjugated on the surface of GMC-CSN-Cxmab-NPs and GMC-CSN-Neu5Ac-Cxmab-NPs [247]. For this 50 µL each of above formulations, 50 µL phosphate buffer saline (PBS) pH 7.4 and 250 µL of Bradford reagent was added to 96-well plate and incubated for 5 min in darkness. PBS pH 7.4 was utilised as a negative control. Then UV-Visible absorbance was recorded on a multi-mode microplate reader at 590 nm (Molecular devices, USA). The Content of Cxmab was measured by using the standard curve of bovine serum albumin [248] using following equation:

$$Content\ of\ Cxmab\ conjugation = \frac{Content\ of\ Cxmab\ in\ NPs - Content\ of\ Cxmab\ in\ blank\ (PBS)}{Content\ of\ Cxmab\ in\ standard\ solution} * 100$$

4.4.4 *In vitro* studies

4.4.4.1 *In vitro* drug release study of gemcitabine from nanoparticles

The release of loaded Gemcitabine (0.5 mg/mL) from nanoformulations was analysed by the dialysis bag diffusion technique at two different pH values; pH 5.5 acetate buffer and pH 7.4 PBS buffer. Before use, the bags were soaked overnight in water. The NPs were retained by the dialysis bag, while the free drug permeated across the membrane into the dissolution media. The dialysis bag was filled with 1 mL of each of NPs separately with both ends clamped together. Each of the bags were put into a beaker having 30 mL of the dissolution media and stirred at 200 rpm at 37 ± 0.5 °C temperature [217]. At prefixed time intervals, 1 mL sample from the each medium was taken with replacement of an equal volume of fresh sample to ensure sink condition [259]. All samples were diluted as required with milli-Q water and passed through a 0.22 micron size syringe filter. The drug content was analysed by RP HPLC method using methanol and water (20:80) as mobile phase.

The drug release data of GMC from CSN-NPs was analysed and the mechanism of drug release kinetics was predicted based on the best fit (chosen based on highest regression coefficient (R^2) values).

4.4.4.2 Cellular Uptake Analysis

Coumarin-6 (C6) loaded nanoformulations were prepared by dissolving coumarin-6 (0.5 mg/mL) in ethanol, 1 mL of which was incubated with 1 mL of each pure GMC, GMC-CSN-NPs, GMC-CSN-Neu5Ac-NPs, GMC-CSN-Cxmab-NPs, and GMC-CSN-Neu5Ac-Cxmab-NPs solution. Cellular uptake of C6-GMC, C6-GMC-CSN-NPs, C6-GMC-CSN-Neu5Ac-NPs, C6-GMC-CSN-Cxmab-NPs and C6-GMC-CSN-Neu5Ac-Cxmab-NPs was investigated on A-549 cells using confocal microscopy. A549 cells at the logarithmic growth phase were seeded on coverslips in 6-well plates at a density of 5×10^4 cells per well, and cultured for 24 h. Subsequently, cells were cultured with DMEM containing C6 labelled pure GMC, GMC-CSN-NPs, GMC-CSN-Neu5Ac-NPs, GMC-CSN-Cxmab-NPs and GMC-CSN-Neu5Ac-Cxmab-NPs (equivalent to 50 μg/mL GMC concentration) respectively, followed by incubation. After incubation, the cells were washed with PBS and fixed with 4% paraformaldehyde solution for 5-10 min. The nuclei were stained with 4′,6-diamidino-2-phenylindole (DAPI) for an additional 15 min. Then the cells were rinsed with PBS and observed under a Zeiss LSM900 confocal laser scanning microscope (Zeiss, Jena, Germany) by adjusting blue signal for DAPI and green signal for C6 at excitation maxima of 405 nm and 488 nm respectively [260]. Fluorescent images were processed using the Zeiss Zen 3.6 blue edition software. The green fluorescent images of all C6-NPs were analysed by image-J software [234]. The total area occupied by C6 in A-549 cells represented in green channel showed cellular uptake of nanoparticles.

4.4.4.3 Cytotoxicity study by MTT assay

The antiproliferative activity of the GMC-CSN-NPs, GMC-CSN-Neu5Ac-NPs, GMC-CSN-Cxmab-NPs, and GMC-CSN-Neu5Ac-Cxmab-NPs was compared with pure GMC by MTT assay in A549 cell line (epithelial lung cancer cell line). Exponentially growing A549 cells were seeded at density of 3×10^4 viable cells/well in 96-well plates in DMEM and incubated for 24 h under controlled environment at 37 °C humidified incubator and 5% CO_2. The cells were individually treated with free GMC and respective GMC loaded CSN-NPs in DMEM medium at concentrations of equivalent amount of GMC ranging from 0.1 to 100 μg/mL for 24 h. Further, 10 μL MTT solution (5 mg/mL in PBS) was added to each well plate and incubated for 4 h leading to formation of purple formazan

crystals through reduction of MTT by viable cells. The formazan crystals were dissolved in 100 µL DMSO, and the absorbance was recorded at 570 nm by microplate reader [235]. The percent cell viability was calculated by:

$$Cell\ viability\ (\%) = \frac{Absorbance\ of\ treated\ cells}{Absorbance\ of\ control\ cells} * 100$$

4.4.4.4 Effect on Metastasis (Wound Healing Assay)

For the wound healing (scratch) assay, A549 cells were seeded at a density of 5×10^4 cells on coverslips in 6-well tissue culture treated plates and incubated overnight at room temperature. Following incubation, each well was scratched with a 100 µL sterile micropipette tip, and the cells were then washed twice with PBS to remove any detached cells. For the next 24 h, the cells were incubated in DMEM with or without nanoformulations. Using an inverted microscope images of the wounds (in triplicate) were taken at 0 h, 24 h, 48 h and 72h. The % wound healing area (% wound closure) associated with cell migration over through the wound was estimated by measuring and comparing the area between wound's edges using Image J software [261].

4.4.4.5 Annexin-V/PI apoptosis assay

The Annexin-V/PI assay was used to study apoptosis by confocal laser scanning microscope (Zeiss, Jena, Germany). In apoptotic cells, phosphatidylserine (PS) is translocated from the interior side to the exterior side of the plasma membrane. Annexin-V specifically classifies apoptotic cells by binding to PS positioned on the exterior side. Briefly A-549 cells were treated with 100 µg/mL pure GMC and equivalent amount of GMC in GMC-CSN-NPs, GMC-CSN-Neu5Ac-NPs, GMC-CSN-Cxmab-NPs, GMC-CSN-Neu5Ac-Cxmab-NPs for 48 h. Treated cells were washed with PBS and suspended in 100 µL of binding buffer (50 mM of HEPES (pH 7.4), 700 mM of NaCl, and 12.5 mM of $CaCl_2$). Samples were incubated with 5 µL of Annexin-V and 2 µL of PI in a dark environment for 20 min at 37 °C. Following incubation, the samples were fixed on a coverslip with 2% formaldehyde and inverted on a glass slide to image the cells. The fluorescence was then measured with a confocal laser scanning microscope by adjusting green channel for Annexin-V and Red channel for propidium iodide (PI) at excitation maxima of 485 nm and 560 nm respectively. Annexin-V/PI positive cells were recognised

as apoptotic cells. The total cell fluorescence of apoptotic cells by Annexin-V/PI were calculated by image J software [234] by using formula:

$$Total\ cell\ Fluorescence\ of\ apoptotic\ cells = Area - (Internal\ Density * Mean)$$

4.4.5 *In vivo* studies

4.4.5.1 Animals

Male Wistar rat weighing 200-250gm and Swiss albino mice weighing 120–150 g were procured from Central Animal House, Department of Pharmaceutical Engineering & Technology, Indian Institute of Technology (Banaras Hindu University), Varanasi-221005, (U.P.), India. The animals were accommodated in clean and sanitary polypropylene cages in a well-ventilated animal house at temperature 25 °C ± 2 °C and fed with pelleted diet and water ad libitum. Animals were placed under a 12 h each light/dark cycle. All animal experiments were done firmly in compliance with the Institutional Animal Ethics Committee's regulations for the control and supervision of experimental animals (2123/GO/Re/S/21/CPCSEA) dated 03/05/2022 under Animal Welfare Section, Government of India, New Delhi.

4.4.5.2 Pharmacokinetic evaluation of gemcitabine

Pharmacokinetic examination of GMC loaded non-targeted (CSN-NPs), targeted (CSN-Neu5Ac-NPs, CSN-Cxmab-NPs, CSN-Cxmab-Neu5Ac-NPs) nanoparticles and native GMC was performed in Wistar rat of body weight between 200-250 g. The animals were distributed into five groups having six animals each. The pure GMC (10 mg/kg) and GMC loaded targeted and non-targeted CSN-NPs containing an equivalent dose (10 mg/kg) of GMC were administered via intravenous injection in tail vein of rat and blood was collected from retro-orbital plexus at different time points. Animals were anesthetized by intra-peritoneal injection of urethane (2 gm/kg) before blood collection [262]. Blood specimens were centrifuged for 15 min at 12000 rpm to collect plasma. To 200 µL of plasma 800 µL of acetonitrile was added to precipitate plasma proteins and extract the drug. Precipitated specimens were centrifuged at 12000 rpm for 15 min and then supernatant was collected. After that acetonitrile was evaporated to get the drug residue. Thereafter, approx. 1 mL of distilled water was added to each

drug sample and analysed by HPLC method. The data was analysed using a non-compartmental model on kinetica 5.0 and GraphPad Software to predict the various pharmacokinetic parameters and plasma drug concentration versus time graph was plotted.

4.4.5.3 *In-vivo* biochemical estimation

Assessment of serum biochemical profile is very essential as it identifies the health state of individual and were estimated for clinical monitoring. After 28 days of different treatment twice weekly (1st and 4th day) via tail vein i.v route with saline control, pure GMC, GMC-CSN-NPs, GMC-CSN-Neu5Ac-NPs, GMC-CSN-Cxmab-NPs and GMC-CSN-Neu5Ac-Cxmab-NPs in the dose range 10 mg/kg body weight of wistar rat, the treated and control animals were anesthetized by intra-peritoneal injection of urethane (2 gm/kg) and blood was collected by from retro-orbital plexus. Blood samples (200 µL) were collected in Eppendorf tubes with heparin and then centrifuged at 5000 rpm for 5 min to obtain serum. Thereafter, Commercial diagnostic kits (Transasia Bio-Medicals Ltd., India) were used to estimate renal function biomarkers (Uric acid, BUN, Creatinine) and hepatic function biomarkers (ALP, ALT and AST) levels from the collected serum samples [263].

4.4.5.4 *In vivo* therapeutic efficacy

The efficacy of different targeted and non-targeted formulations of CSN-NPs to down-regulate B[a]P-induced lung cancer was assessed in male Swiss albino mice. Briefly, the mice were randomly assigned to seven groups having six animals per group. Group I (negative control) received olive oil orally twice a week during the experimentation, Group II (model control) animals administered B[a]P (50 mg/kg) dissolved in olive oil, twice weekly (1st and 4th day), for a period of 4 weeks via oral gavage. Group III (drug control), group IV (GMC-CSN-NPs), group V (GMC-CSN-Neu5Ac-NPs), group VI (GMC-CSN-Cxmab-NPs) and group VII (GMC-CSN-Neu5Ac-Cxmab-NPs) with an equivalent 10 mg/kg dose of GMC in each group was administered intravenously through tail vein two times a week respectively, starting from 4th week up to 8th weeks after B(a)P treatment in respective groups. At the end of 16th week, intraperitoneal injection of urethane (2 g/kg bodyweight) was used to anaesthetize and sacrifice all surviving animals. Then , lungs from all the groups was immediately harvested, fixed with 10% formalin solution, processed for paraffin block sectioning

(5µm thick), and mounted over glass slides followed by hematoxylin and eosin (H&E) staining to observe the tissue sections under optical microscope. The optical images were processed using Image J software to determine the number of proliferated lung cancerous cells. Next, the six lung cancer-bearing mice in each group were evaluated in the survival study by Kaplan-Meier graphical model [3,234].

4.5 Results and discussion

4.5.1 Optimization of chimeric mAb conjugated chitosan nanoparticles

For optimization of mAb concentration, seven experiments were proposed by Box-Behnken design using one-factor approach by Design Expert software. As per the design in order to minimise experimental errors, five experiments were classified as major, while the other two were marked as repeating experiments as shown in **Table 4.3.**

Table 4.3 Experiments designed by Design-Expert 7.0 to optimize the amount of monoclonal antibody cetuximab (Cxmab) and; the results of the amount of Cxmab conjugated to the GMC-CSN-NPs in each experiment.

Runs	Amount of Cxmab (mg)	Conjugated Cxamb (%)
1	1.00	40.34
2	1.75	63.21
3	2.00	65.34
4	1.00	35.56
5	1.50	55.34
6	**2.00**	**72.13**
7	1.25	43.17

***** Bold values indicate optimized values obtained by using Design Expert software.

Response surface data of all experimental trials were best fitted to a quadratic model. The extent of conjugation of Cxmab to GMC-CSN-NPs varied 35.56% to 72.13%. The following full model polynomial equation was obtained in terms of coded factors; concentration of cetuximab (A):

Conjugated Cxmab = +53.58+15.91* A

The value of the coefficient of correlation (R^2) for conjugated Cxmab indicated a good fit, and the predicted R^2 (0.9101) was found to be in reasonable agreement with adjusted R^2 (0.9518).

Adeq Precision" measures the signal to noise ratio, a ratio greater than 4 is desirable. The Adeq Precision ratio of conjugated Cxmab was 19.271 indicating an adequate signal.

Based on the overall desirability analysis, predicted factor (i.e. amount of Cxmab) was found to be 2 mg, and the predicted response (i.e. extent of conjugation of Cxmab) was 69.49%, with the overall desirability value being 0.928. The optimized formulation prepared using the predicted factors exhibited 72.13% conjugation of Cxmab, which was very close to predicted value.

4.5.2 Physiochemical characterization of nanoparticles

The physiochemical characteristics of NPs has been shown in **Table 4.4**. The particle size analysis revealed that all NPs were in the size range between 100 to 200 nm. The particle size data indicated that the attachment of Neu5Ac and Cxmab to the surface of NPs results in increase in size of the targeted NPs. Furthermore, the PDI of NPs was found to be in the range of 0.2-0.3, indicating homogeneously dispersed particles with a smooth surface. NPs with values of PDI and size both being less than 0.5 and 200 nm respectively are mono-disperse and ideal for drug delivery to cancerous tissues [264].

Change in Zeta potential helped to suggest the coating of Neu5Ac and EGFR antibody (Cxmab) on the surface of CSN-NPs. GMC-CSN-NPs were found to have a surface charge of 52.83±1.90 mV, which decreased to 41.7±2.66 mV following conjugation with Neu5Ac on CSN-NPs in GMC-CSN-Neu5Ac-NPs, Contrarily, it was further lowered in GMC-CSN-Cxmab-NPs and GMC-CSN-Neu5Ac-Cxmab-NPs to 36.46±1.05mV and 28.73±3.72mV, respectively. Particularly, the positive zeta potential is advantageous for electrostatic attraction with oppositely charge ligands [265]. Further, the positive charge on targeted NP decreased because of electrostatic attraction between negative surface charges associated with Neu5Ac and cetuximab and positive charge on CSN-NPs (**Figure 4.2).**

Table 4.4 Physiochemical characterization of non-targeted and targeted chitosan nanoparticles.

Nanoformulations	Particle size (nm) (Mean ± SD)*	PDI (Mean ± SD)*	Zeta potential (mV) (Mean ± SD)*	Entrapment efficiency (Mean ± SD)*
GMC-CSN-NPs	140.8±7.53	0.23±0.06	52.83±1.90	69.33±2.49
GMC-CSN-Neu5Ac-NPs	162.73±7.24	0.22±0.06	41.7±2.66	65.78±1.66
GMC-CSN-Cxmab NPs	175.7±4.38	0.28±0.09	36.46±1.05	64.27±1.20
GMC-CSN-Neu5Ac-Cxmab-NPs	186.03± 8.10	0.26±0.01	28.73±3.72	62.86±1.60

***** Results presented as mean ± standard deviation, n=3

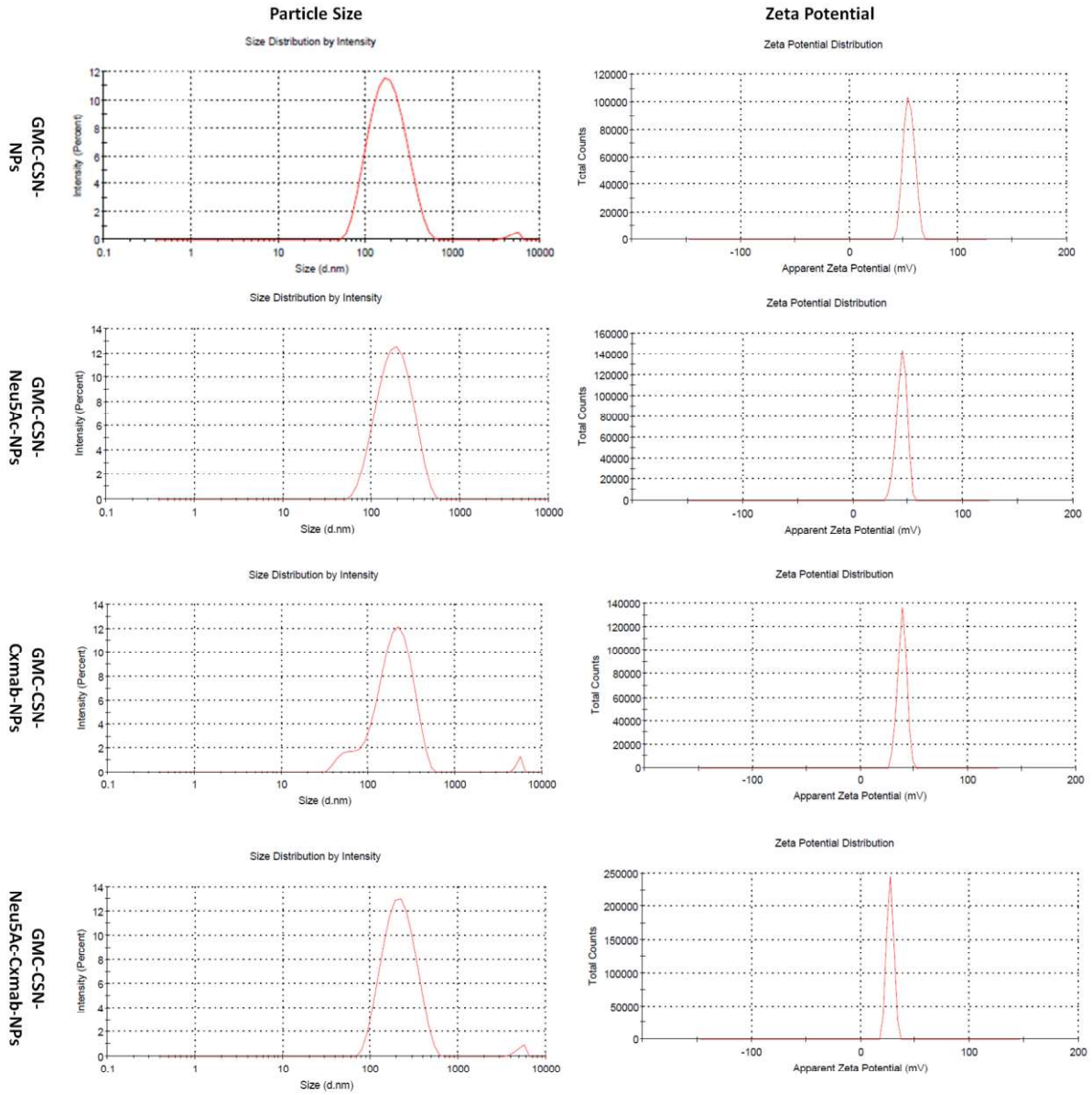

Figure 4.2 Average size and zeta potential distribution of GMC-CSN-NPs, GMC-CSN-Neu5Ac-NPs, GMC-CSN-Cxmab-NPs, GMC-CSN-Neu5Ac-Cxmab-NPs measured by DLS.

4.5.3 Determination of entrapment efficiency (% EE)

% EE of gemcitabine loaded non-targeted (GMC-CSN-NPs) and targeted (GMC-CSN-Neu5Ac-NPs, GMC-CSN-Cxmab-NPs, GMC-CSN-Neu5Ac-Cxmab-NPs) nanoparticles was 69.33±2.49%, 65.78±1.66%, 64.27±1.20%and 62.86±1.60% respectively. Targeted nanoparticles exhibited a somewhat lower % EE than non-targeted NPs probably due to surface modification of targeted NPs with Neu5Ac and EGFR targeting antibody (Cxmab).

4.5.4 Morphological analysis of nanoparticles

Morphological analysis of CSN-NPs has been shown in **Figure 4.3**. SEM was initially employed to evaluate the NPs morphology (size and shape).The SEM analysis revealed that the NPs exhibited uniform size with well dispersed, diameters in the range of 200 nm. These particles showed spherical shape, which was further verified by TEM imaging.

TEM images of the NPs showed distinct, monodisperse, spherical particles without agglomeration (Scale bar 200 nm). The TEM images clearly demonstrated that non-targeted NPs exhibited dark core ascribed to the chitosan matrix, whereas targeted NPs displayed dark core surrounded by a bright layer of targeting moieties. Particle size measurement from dynamic light scattering (DLS) analyses correlated identically with that obtained from SEM and TEM observations.

Selected area diffraction (SAD) pattern showed separate ring pattern in case of GMC-CSN-NPs which suggest crystalline nature while the SAD images of GMC-CSN-Neu5Ac-NPs, GMC-CSN-Cxmab-NPs and GMC-CSN-Neu5Ac-Cxmab-NPs had diffused rings which represent an amorphous background.

The surface topography and particle size of CSN NPs was examined by 2D and 3D AFM topographic images, respectively. In these images, individually separated spherical, smooth surfaced NPs, below 200 nm in size were observed. These images illustrated the appearance of individual NPs. Furthermore, aggregation of nanoparticles was also identified. The aggregation might be the result of sample-drying, caused by reduction in solvent volume around the NPs. The size of the NPs acquired

by AFM was somewhat lower than the corresponding size recorded by DLS [266]., The topographical, geometrical parameters/size, and roughness influence the cellular behaviour and cellular adhesion characteristics of the NPs. The roughness of the NPs enables the cells to groove deeply into the membrane, influencing viable cell movement and adherence. In another research, it was reported that increase in surface roughness reduce cell adherence and proliferation [267].

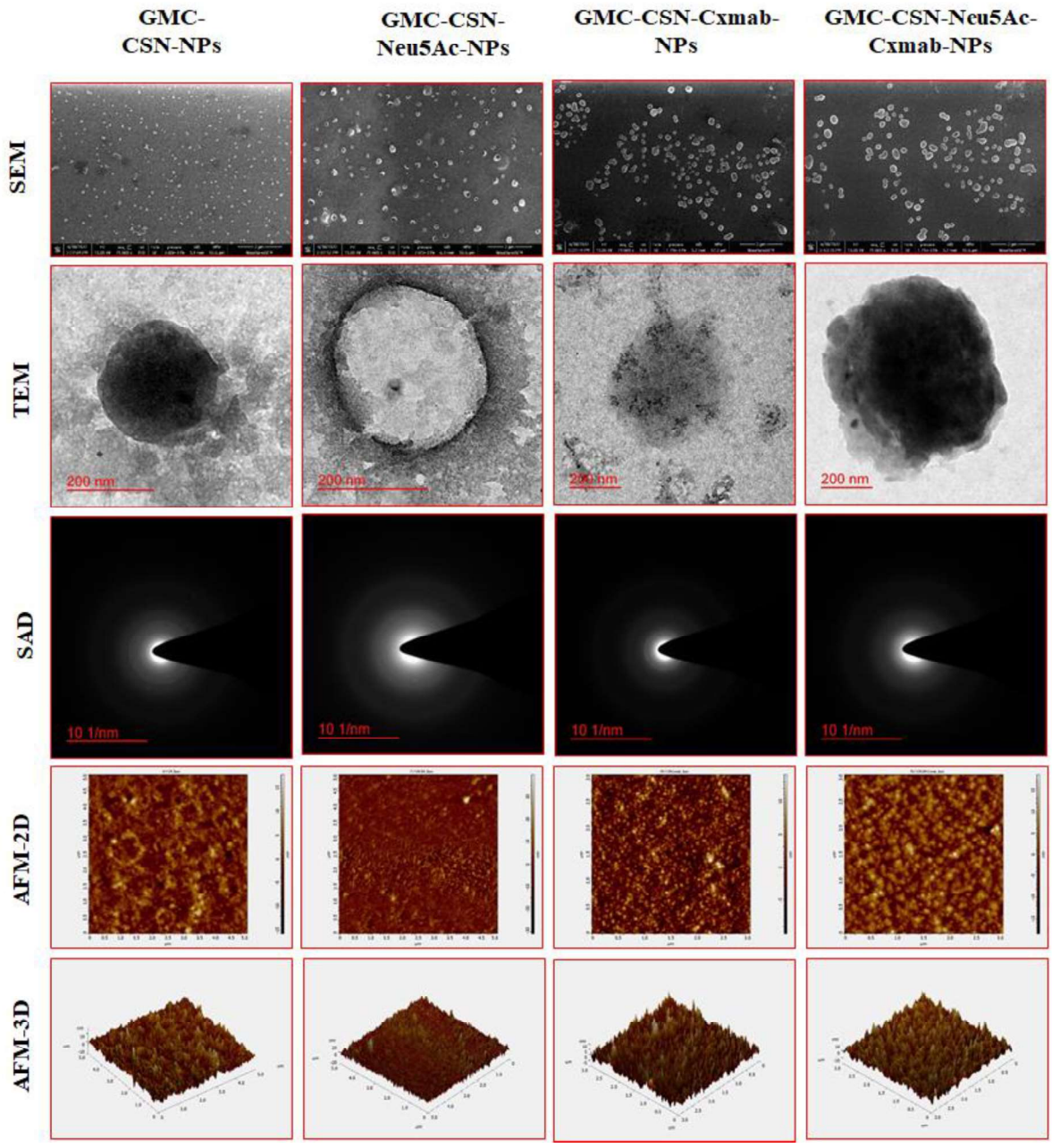

Figure 4.3 Representative images of morphological analysis of non-targeted and targeted chitosan nanoparticles.

4.5.5 Evaluation of surface chemistry of nanoparticles

The XPS spectra of CSN-NPs exhibited typical peaks of atoms C, N, and O, as shown in **Figure 4.4 A**. The proportions of N1s, O1s and C1s observed in GMC-CSN-NPs were 6.29%, 29.98% and 63.72% respectively, whereas for GMC-CSN-Neu5Ac-NPs, these values were 6.6%, 28.2% and 65.2% respectively. The rise in the proportion of N1s and C1s in GMC-CSN-Neu5Ac-NPs can be attributed to the presence of Neu5Ac on the surface of NPs. The successful coating of Cxmab by electrostatic interaction on GMC-CSN-NPs and GMC-CSN-Neu5Ac-NPs was also verified by the XPS analysis. The proportion of N1s, O1s and C1s in GMC-CSN-Cxmab-NPs was 13.6%, 20.82% and 65.57% respectively, while for GMC-CSN-Neu5Ac-Cxmab-NPs, the proportions were 11.5%, 24.74% and 63.7% respectively. The rise in proportion of nitrogen in GMC-CSN-Cxmab-NPs (13.6%) and GMC-CSN-Neu5Ac-Cxmab-NPs (11.5%) was due to coating of Cxmab on GMC-CSN-NPs (6.29%) and GMC-CSN-Neu5Ac-NPs (6.6%) respectively, as Cxmab has high proportion of nitrogen atoms. The XPS spectra shows the identifiable intensities of nitrogen, oxygen, and carbon due to presence of Cxmab and Neu5Ac on the surface of GMC-CSN-NPs. An extra peak detected near about 500 eV is specific for Na KLL (Na 2s) that might be related to the sodium tripolyphosphate, the cross linker used in the formulation of CSN-NPs.

4.5.6 Solid state characterization of nanoparticles

4.5.6.1 XRD analysis

The findings of an XRD study of pure GMC, GMC loaded non-targeted, and targeted formulations have been shown in **Figure 4.4 B**. The appearance of large number of peaks in the XRD spectra of pure GMC shows its crystalline character while these peaks were missing in the spectrum of non-targeted (GMC-CSN-NPs) and targeted CSN-NPs (GMC-CSN-Neu5Ac-NPs, GMC-CSN-Cxmab-NPs and GMC-CSN-Neu5Ac-Cxmab-NPs). This results further suggest that GMC was entrapped in an amorphous form with in the nanoformulations.

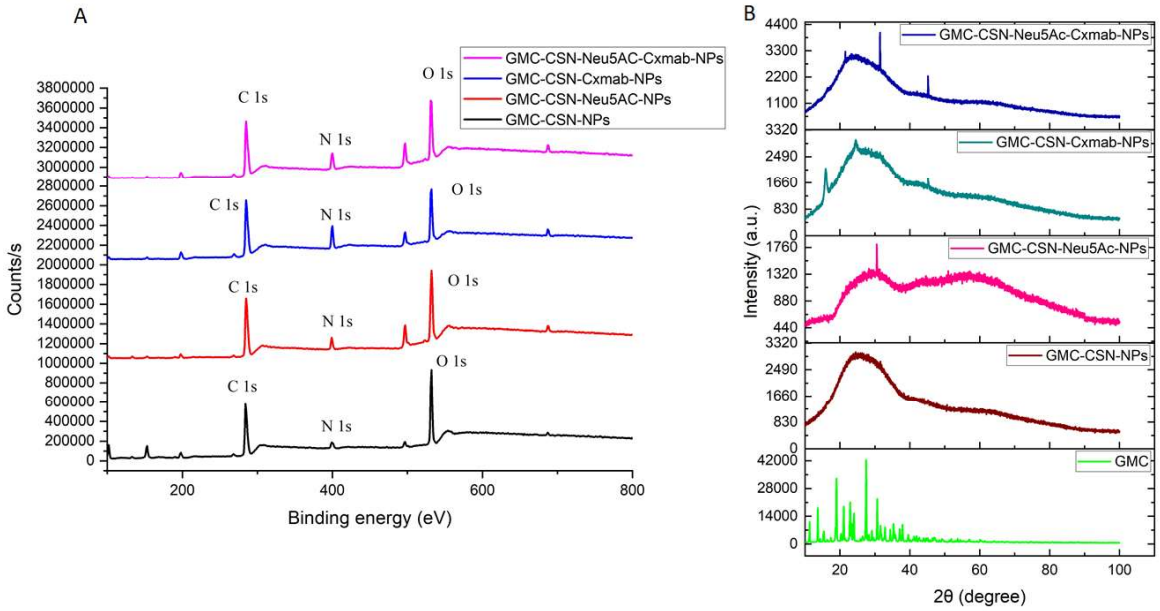

Figure 4.4 A. XPS spectra of non-targeted and targeted CSN-NPs for identification of Neu5Ac and Cxmab coating onto CSN-NPs. B. XRD overlay spectrum of pure GMC, non-targeted and targeted CSN-NPs to qualitatively evaluate entrapment of GMC into CSN-NPs.

4.5.6.2 DSC analysis

The DSC analysis shown in **Figure 4.5 A** was performed to verify the physical state of the GMC within the targeted and non-targeted CSN-NPs. The DSC thermogram of the GMC showed an endothermic peak at 261 °C (also, its melting point), suggesting its crystalline nature. However, prepared CSN-NPs exhibited no characteristic peak of GMC indicating encapsulation of GMC in CSN-NPs in amorphous form.

4.5.6.3 FTIR analysis

The drug entrapment in targeted and non-targeted CSN-NPs was further confirmed by FTIR analysis. The major characteristic of GMC was around 3400 cm^{-1} (O-H stretching) attributed to the hydroxyl groups present in pentose sugar moiety of GMC, 3250 cm^{-1} (-NH_2 stretching), 1675.44 cm^{-1} (N-H bending) owing to free amino group, 1542 cm^{-1} (N-H bending) due to amide group, 1382 cm^{-1} (C-N stretch) for the pyrimidine ring and 1050 cm^{-1} (C-O-C stretching). The major peaks of gemcitabine disappeared in GMC encapsulated targeted and non-targeted CSN-NPs as shown in **Figure 4.5 B**. The results suggest that GMC was successfully entrapped in the polymeric matrix of CSN-NPs.

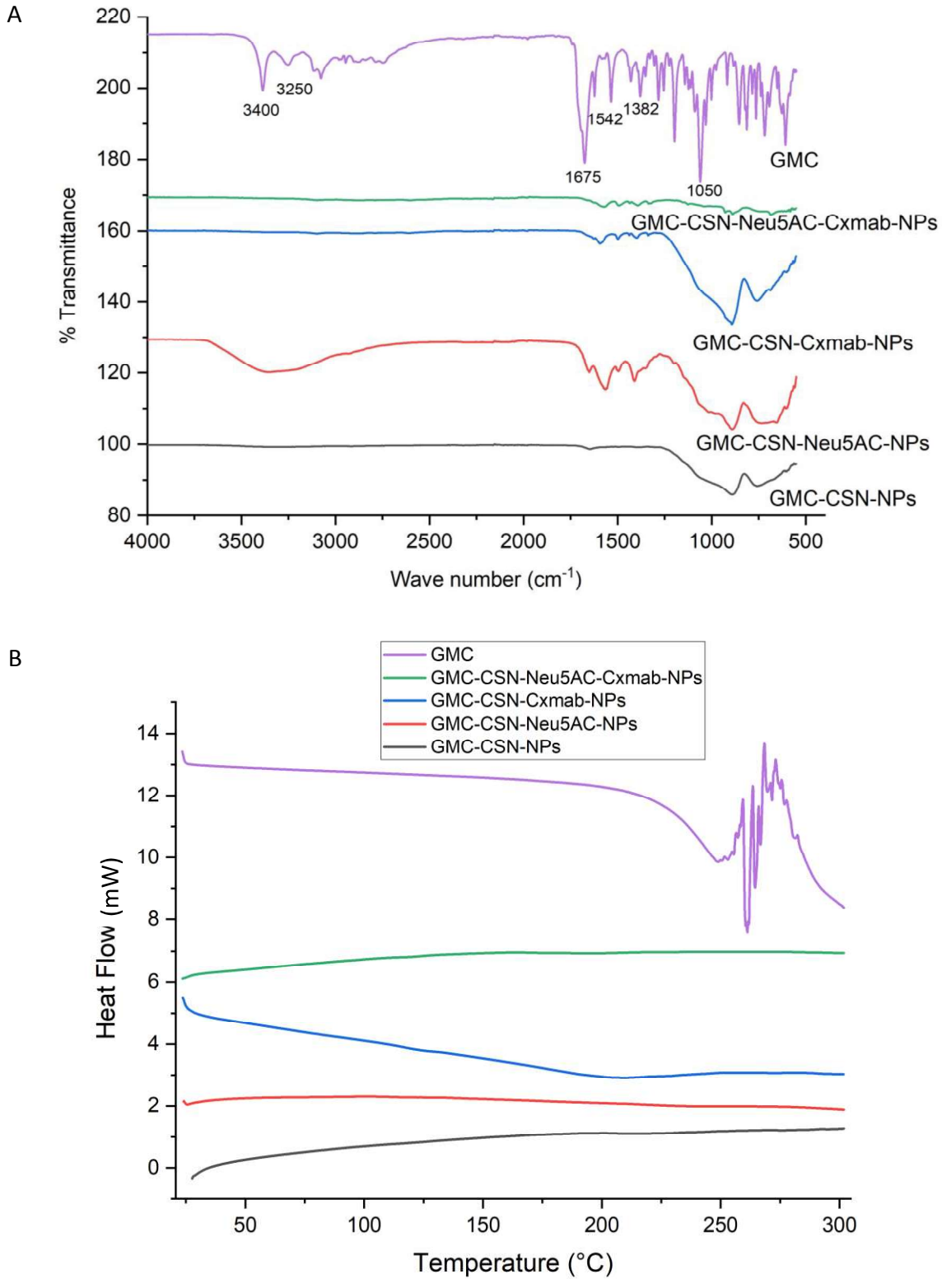

Figure 4.5 A. DSC B. FTIR spectra of gemcitabine and gemcitabine encapsulated targeted and non-targeted chitosan nanoparticles.

4.5.7 Estimation of amount of 5-N-acetyl-neuraminic acid conjugated in CSN-Neu5AC conjugate and on to surface of nanoparticles

Approximately, 78.50 ±3.32% of Neu5Ac content was quantified in CSN-Neu5Ac conjugates and 67.22 ± 2.36% of Neu5Ac in GMC-CSN-Neu5Ac-NPs and 58.46 ± 2.20% in GMC-CSN-Neu5Ac-Cxmab-NPs. Reduction in Neu5Ac content in case of GMC-CSN-Neu5Ac-Cxmab-NPs may due to the conjugation of cetuximab along with Neu5Ac.

4.5.8 Estimation of cetuximab concentration conjugated on surface of nanoparticles

The amount of Cxmab conjugated on the surface of GMC-CSN-Cxmab-NPs and GMC-CSN-Neu5Ac-Cxmab-NPs was calculated by Bradford assay. The results showed that nearly 72.94 ± 3.47% of Cxmab surface conjugation was achieved in GMC-CSN-Cxmab-NPs. In GMC-CSN-Neu5Ac-Cxmab-NPs, it was 63.20 ± 2.12%. Low level of Cxmab conjugation was observed in GMC-CSN-Neu5Ac-Cxmab-NPs probably due to the presence of Neu5Ac residues along with Cxmab.

4.5.9 *In vitro* studies

4.5.9.1 *In vitro* drug release study

GMC showed pH dependent release from CSN-NPs. CSN dissolves in acidic solutions with pKa less than 6.3 [268]. In acidic conditions, protonation of NH_2 groups results in the formation of NH_3^+. The presence of positively charged NH_3^+ groups generates repulsion between the CSN chains resulting in swelling of the NPs, allowing the branches of polymeric network to open and release the encapsulated drug [269]. The release of gemcitabine from the non-targeted and targeted CSN-NPs in acetate buffer at pH 5.5 and PBS buffer at pH 7.4 have been mentioned in **Figure 4.6**. CSN-NPs showed 48.59 ± 3.00% and 33.89 ± 1.61% burst release during the first 12 h at pH 5.5 and 7.4, respectively. This “burst effect”, occurs due to desorption of GMC, confined on the surface of NPs. After 12 h, all formulations showed a slow drug release pattern (sustained release), probably due to the slower migration of GMC entrapped within the mesh cavities of NPs.

The drug release was studied at pH of 5.5, which mimics endo/lysosomal pH [270]. At this pH, significant proportion of the loaded drug is expected to release inside the cells. Rate of drug release was noticeably higher at pH 5.5 (85.43± 7.87%) as compared to pH 7.4 (56.19± 2.27%). Since cancerous cells have an acidic microenvironment, the release of drug from CSN-NPs is anticipated to be higher at this pH in cancerous cells. The amount (%) of GMC released from non-targeted (GMC-CSN-NPs) and targeted (GMC-CSN-Neu5Ac-NPs, GMC-CSN-Cxmab-NPs, GMC-CSN-Neu5Ac-Cxmab-NPs) CSN-NPs in acetate buffer (pH 5.5) after 72 h, was 91.97 ± 1.39%, 88.69 ± 2.07%, 87.05 ± 2.18%, and 74.02 ± 3.24% respectively. Additionally, the release of GMC from CSN-NPs was also assessed in PBS (pH 7.4) at 37 °C, which simulates the physiological condition [270] and it was observed that after 72 h the cumulative percentage release from non-targeted (GMC-CSN-NPs) and targeted (GMC-CSN-Neu5Ac-NPs, GMC-CSN-Cxmab-NPs, GMC-CSN-Neu5Ac-Cxmab-NPs) CSN-NPs in PBS buffer (pH 7.4) was 59.47 ± 2.35%, 54.68 ± 2.64%, 57.04 ± 2.85%, and 53.57 ± 3.05% respectively. At neutral pH, GMC-loaded CSN-NPs were extremely stable. These results indicate that the release of GMC from the GMC-loaded with or without ligand modified CSN-NPs show a pH-dependent release and can be potentially beneficial for cancer treatment. As compared to conventional systemic delivery of GMC, this approach may result in minimal adverse effects because of negligible release of drug from the NPs in healthy tissues.

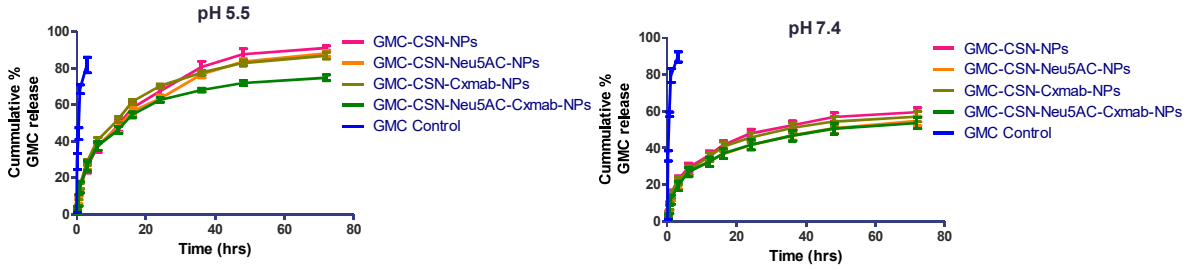

Figure 4.6 Release profiles GMC from non-targeted (GMC-CSN-NPs) and targeted (GMC-CSN-Neu5Ac-NPs, GMC-CSN-Cxmab-NPs, GMC-CSN-Neu5Ac-Cxmab-NPs) CSN-NPs in acetate buffer (pH 5.5) and PBS buffer (pH 7.4). The data has been represented as mean ±SD (n = 3).

Table 4.5 *In vitro* drug release kinetics (with regression coefficient (R^2) at pH 5.5 and pH 7.4.

pH	Drug release kinetics models	GMC-CSN-NPs (R^2)	GMC-CSN-Neu5Ac-NPs (R^2)	GMC-CSN-Cxmab-NPs (R^2)	GMC-CSN-Neu5Ac-Cxmab-NPs (R^2)
5.5	Zero order	0.585	0.551	0.466	0.389
	First order	0.965	0.937	0.934	0.837
	Higuchi	0.963	0.958	0.928	0.907
	Korsmeyer-Peppas	0.982	0.985	0.970	0.969
	Hixon-Crowell	0.938	0.899	0.891	0.759
	Peppas-Sahlin	0.998	0.997	0.996	0.997
7.4	Zero order	0.343	0.356	0.326	0.378
	First order	0.675	0.635	0.647	0.650
	Higuchi	0.902	0.907	0.896	0.911
	Korsmeyer-Peppas	0.983	0.987	0.982	0.982
	Hixon-Crowell	0.586	0.556	0.558	0.572
	Peppas-Sahlin	0.997	0.996	0.997	0.997

The drug release from CSN-NPs at pH 5.5 and 7.4 follows Peppas-Sahlin model as shown in **Table 4.5**. The rate equation of Peppas-Sahlin model has been given below:

$$Q_t = k_1 t^m + k_2 t^{2m}$$

Where; Q_t = fraction of drug released at time t, k_1 = Fickian diffusion constant; k_2 = macromolecular relaxation constant; m = diffusional exponent.

Based on Peppas-Sahlin best fitting values which are in the range of $0.5 < m < 0.6$ for all formulations and showed anomalous transport mechanism of drug release. Additionally the values of k_1 is greater than k_2, and as the pH increase k_1 value decrease, suggesting a decrease in Fickian diffusion as shown in **Table 4.6**. As a result, the role of Fickian diffusion in the release of GMC is less significant at pH 7.4. However, both Fickian diffusion rate and polymer chain relaxation mechanism are prominent and influence the release of GMC from CSN-NPs at pH 5.5 [271].

Table 4.6 Peppas Sahlin drug kinetics model indicating the best-fit values for chitosan nanoparticles.

Parameter	GMC-CSN-NPs (pH 5.5)	GMC-CSN-NPs (pH 7.4)	GMC-CSN-Neu5Ac-NPs (pH 5.5)	GMC-CSN-Neu5Ac-NPs (pH 7.4)	GMC-CSN-Cxmab-NPs (pH 5.5)	GMC-CSN-Cxmab-NPs (pH 7.4)	GMC-CSN-Neu5Ac-Cxmab-NPs (pH 5.5)	GMC-CSN-Neu5Ac-Cxmab-NPs (pH 7.4)
k_1	13.994	13.520	14.950	13.055	15.704	13.666	15.326	11.906
k_2	-0.498	-0.817	-0.622	-0.755	-0.715	-0.815	-0.790	-0.666
m	0.603	0.483	0.553	0.456	0.574	0.481	0.548	0.495

4.5.9.2 Cellular Uptake Analysis

Confocal microscopy was employed to monitor the cellular uptake of C6-labeled pure GMC, non-targeted and targeted CSN-NPs in A549 lung cancer cells. After 24 h incubation, the DAPI stained nuclei showed blue fluorescence enclosed by the green fluorescence of C6 labelled GMC-CSN-NPs, GMC-CSN-Neu5Ac-NPs, GMC-CSN-Cxmab-NPs and GMC-CSN-Neu5Ac-Cxmab-NPs, which demonstrate that a significant portion of the NPs could be incorporated into the cytoplasm **(Figure 4.7 A)**. Based on green fluorescence intensity the cellular uptake of targeted CSN-NPs was compared to the non-targeted CSN-NPs and pure GMC. The fluorescence intensity was determined by measuring the total area occupied by C6 in A-549 cells using image-J software (**Figure 4.7 B)**. The total area occupied by green fluorescent images of C6 labelled pure GMC, GMC-CSN-NPs, GMC-CSN-Neu5Ac-NPs, GMC-CSN-Cxmab-NPs and GMC-CSN-Neu5Ac-Cxmab-NPs was 0.33±0.24, 0.86±0.25, 2.00±0.30, 2.69±0.22 and 3.36±0.155. The total area occupied by C6 differed non-significantly ($p > 0.05$) with pure GMC in comparison to non-targeted NPs (GMC-CSN-NPs) but was significantly higher ($p < 0.001$) with EGFR and glycan receptor targeted NPs (GMC-CSN-Neu5Ac-Cxmab-NPs), EGFR targeted NPs (GMC-CSN-Cxmab-NPs) ($p < 0.001$) and Neu5Ac targeted NPs (GMC-CSN-Neu5Ac-NPs) ($p < 0.01$). The total area occupied by C6 varied significantly among the groups C6-GMC-CSN-Neu5Ac-NPs and C6-GMC-CSN-Neu5Ac-Cxmab-NPs *($p < 0.05$),* C6-GMC-CSN-Neu5Ac-NPs and C6-GMC-CSN-Neu5Ac-Cxmab-NPs (*$p < 0.001$, C6*-GMC-CSN-Cxmab-NPs and C6-GMC-CSN-Neu5Ac-Cxmab-NPs *($p < 0.05$).* Results revealed that the cellular uptake was improved progressively by EGFR and glycan receptor targeted CSN-NPs suggesting the role of

receptor mediated endocytosis. With C6-GMC-CSN-Neu5Ac-Cxmab-NPs, the green fluorescence became more intense and evenly distributed throughout the entire area of cytoplasm as compared to GMC-CSN-Neu5Ac-NPs, GMC-CSN-Cxmab-NPs, non-targeted CSN-NPs and pure GMC. Thus, both EGFR and glycan receptor targeted nanoparticles enter and accumulate into the cells showing higher cellular uptake.

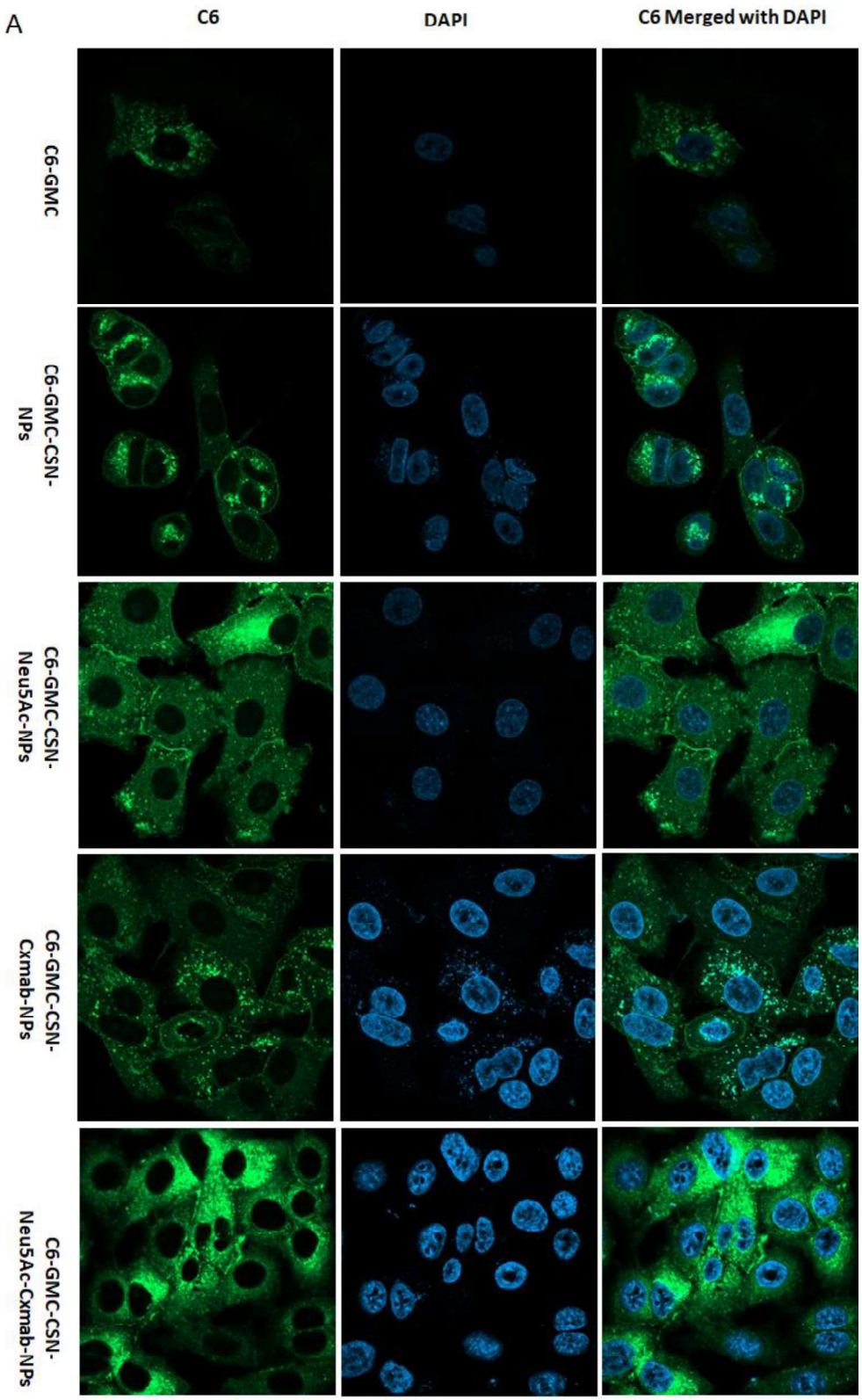
A
C6
DAPI
C6 Merged with DAPI
C6-GMC
C6-GMC-CSN-NPs
C6-GMC-CSN-Neu5Ac-NPs
C6-GMC-CSN-Cxmab-NPs
C6-GMC-CSN-Neu5Ac-Cxmab-NPs

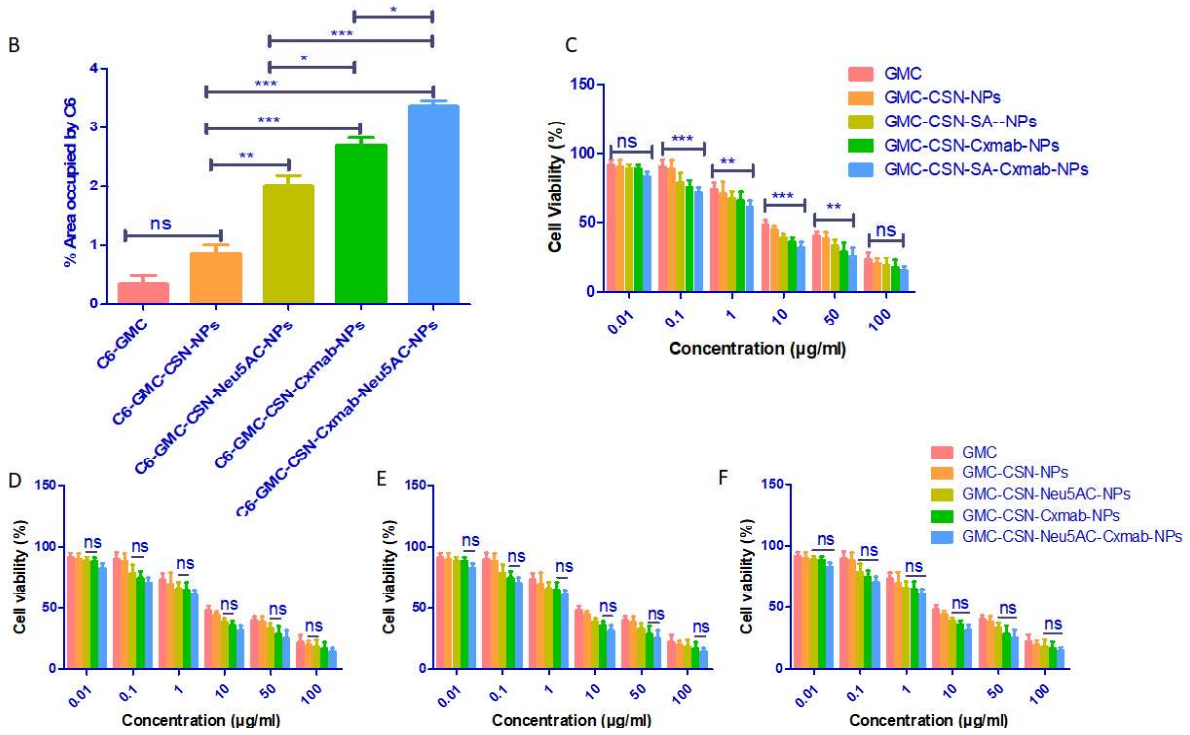

Figure 4.7 A. Cellular uptake study of coumarin-6 (C6) labelled pure GMC, GMC-CSN-NPs, GMC-CSN-Neu5Ac-NPs, GMC-CSN-Cxmab-NPs and GMC-CSN-Neu5Ac-Cxmab-NPs with A-549 cells. B. Total area occupied by C6 in A-549 lung cancer cells by pure GMC, non-targeted and targeted CSN-NPs as analysed by Image-J software. C. % Cell viability of pure GMC & GMC-CSN-Neu5Ac-Cxmab-NPs after 24 h of incubation. D. % Cell viability of GMC-CSN-Neu5Ac-NPs & GMC-CSN-Cxmab-NPs after 24 h of incubation. E. % Cell viability of GMC-CSN-Cxmab-NPs & GMC-CSN-Neu5Ac-Cxmab-NPs after 24 h of incubation. F. % Cell viability of GMC-CSN-Neu5Ac-NPs & GMC-CSN-Neu5Ac-Cxmab-NPs after 24 h of incubation. *($^{*}p < 0.05$), ($^{**}p < 0.01$), ($^{***}p < 0.001$)* were considered as statistically significant and *($p > 0.05$)* non-significant (ns).

4.5.9.3 Cytotoxicity study by MTT assay

The cytotoxicity of GMC loaded non-targeted (GMC-CSN-NPs) and EGFR and glycan receptor targeted (GMC-CSN-Neu5Ac-NPs, GMC-CSN-Cxmab-NPs and GMC-CSN-Neu5Ac-Cxmab-NPs) CSN-NPs were evaluated on A-549 cells. The therapeutic effectiveness of drug loaded NPs is determined by their cellular uptake , intracellular distribution, active targeting ability, and most crucially the dose of the drug released inside the cell from the encapsulated NPs [272]. The percent cell viability of respective nanoformulations in comparison with pure GMC at different concentrations of GMC for 24 h has been illustrated graphically **(Figure 4.7 C)**. The percent cell viability of GMC-CSN-Neu5Ac-Cxmab-NPs was lesser in comparison to GMC-CSN-Neu5Ac-NPs, GMC-CSN-Cxmab-NPs, GMC-CSN-NPs and pure GMC. The percent cell viability on incubation with GMC-

CSN-Neu5Ac-Cxmab-NPs was significantly reduced at concentration 0.1 µg/mL ($p < 0.001$), 1 µg/mL ($p < 0.01$), 10 µg/mL ($p < 0.001$), and 50 µg/mL ($p < 0.01$) than pure GMC. IC50 value was calculated to quantitate the chemotherapeutic effect of specific nanoformulations in terms of cytotoxicity. The percent cell viability differ non-significantly among the groups GMC-CSN-Neu5Ac-NPs and GMC-CSN-Neu5Ac-Cxmab-NPs *($p < 0.05$),* GMC-CSN-Neu5Ac-NPs and GMC-CSN-Neu5Ac-Cxmab-NPs *($p < 0.05$),* GMC-CSN-Cxmab-NPs and GMC-CSN-Neu5Ac-Cxmab-NPs *($p < 0.05$)* **(Figure 4.7 D, E & F)**.. The IC50 value of pure GMC, GMC-CSN-NPs, GMC-CSN-Neu5Ac-NPs, GMC-CSN-Cxmab-NPs and GMC-CSN-Neu5Ac-Cxmab-NPs was 14.47±1.45, 10.15±2.55, 8.763±1.90, 6.861±1.84, and 4.096±1.51 µg/mL, respectively after 24 h of incubation. Thus, it is noticeably evident that on increase in the drug concentration from 0.01 µg/mL to 100 µg/mL of various GMC loaded Cxmab and Neu5Ac decorated CSN-NPs, there is enhancement in the cytotoxicity in lung cancer A-549 cells (which overexpress EGFR and glycan receptors). This could be due to the higher delivery of GMC in the cancerous tissues by higher cellular uptake and via receptor mediated endocytosis of targeted CSN-NPs. These results suggest that EGFR and glycan receptor targeted CSN-NPs can significantly enhance the chemotherapeutic effect of GMC on A-549 cells.

4.5.9.4 Effect on Metastasis

Wound healing assays have extensively been used to estimate the efficacy of the treatment groups on cell migration that is an essential stage for tumor metastasis [273]. Wound-healing assay was carried out to describe the growth inhibitory effect of targeted and non-targeted CSN-NPs. Targeted CSN-NPs exhibit higher growth inhibitory effect on cell migration. The A-549 cells were scratched for creation of wound at 0h (pre-treatment), and movement of cells was detected after 12h, 48 h and 72 h resulting in wound closure (i.e., shrinkage in width of wound) in media **(Figure 4.8 A, B)**. The GMC-CSN-Neu5Ac-Cxmab-NPs treated A-549 cells migrated less as compared to GMC-CSN-Cxmab-NPs, GMC-CSN-Neu5Ac-NPs, GMC-CSN-NPs treated and control (pure GMC) ($p < 0.001$), indicating that targeted CSN-NPs inhibit the migration of A549 cells. The results indicate that GMC-CSN-

Neu5Ac-Cxmab-NPs have an enhanced ability to prevent lung cancer metastasis in comparison to other treatment groups.

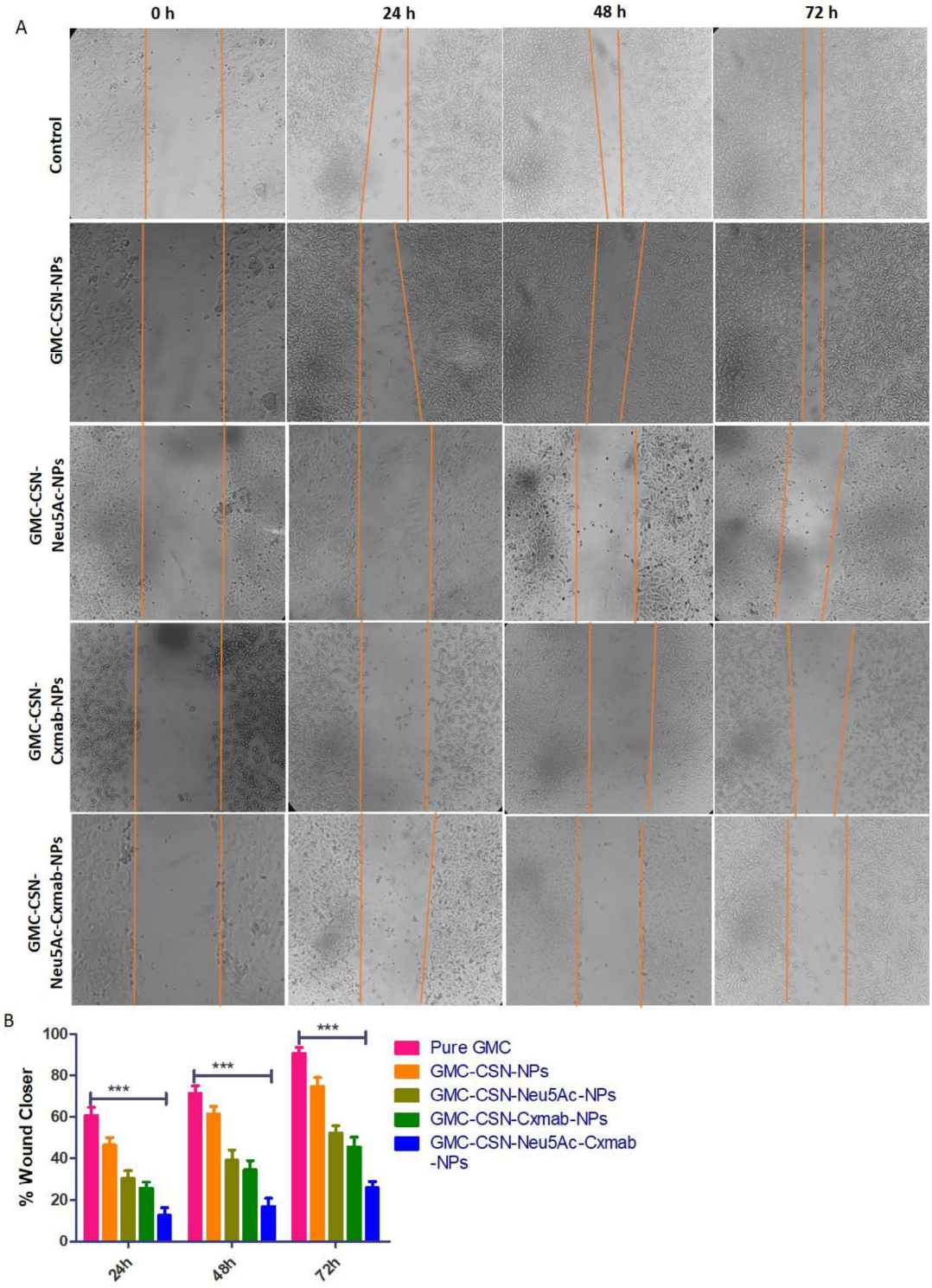

Figure 4.8 A. Light microscopic images of metastatic effect on A549 cells after 0h, 24h, 48h and 72 h of treatment with control (pure GMC), non-targeted (GMC-CSN-NPs) and targeted (GMC-CSN-Neu5Ac-NPs, GMC-CSN-Cxmab-NPs, GMC-CSN-Neu5Ac-Cxmab-NPs) CSN-NPs. B. Quantitative illustration of wound healing of A549 cells treated with different groups expressed as %wound

closure at specified time. The %wound closure of GMC-CSN-Neu5Ac-Cxmab-NPs was significantly ($p < 0.001$) less than pure GMC. Data represented as mean ± SD (n=3). Statistically significant (* $p < 0.05$), (** $p < 0.01$), (*** $p < 0.001$).

4.5.9.5 Annexin-v/PI apoptosis assay

The apoptosis inducing capability of GMC is a significant factor for tumor growth inhibition in NSCLC. Therefore, Annexin-V/PI stained A-549 cells treated with GMC loaded NPs were also examined for cellular apoptosis. Cells that with bound annexin-V showed green staining with externalized phosphatidyl serine (PS) on plasma membrane and the cells which lost membrane integrity exhibited red staining (PI) throughout the nucleus. After treatment, GMC-CSN-Neu5Ac-Cxmab-NPs treated cells demonstrated higher green and red fluorescence due to distorted morphology and appearance of more apoptotic bodies as compared to GMC-CSN-NPs, GMC-CSN-Neu5Ac-NPs, GMC-CSN-Cxmab-NPs and pure GMC **(Figure 4.9 A).**Total cell fluorescence of Annexin-V/PI stained apoptotic cells was performed using ImageJ software which indicated significantly higher apoptotsis in GMC-CSN-Neu5Ac-Cxmab-NPs treated cells as compared to other groups. The number of apoptotic cells in non-targeted (GMC-CSN-NPs) nanoparticles was non-significantly higher ($p > 0.05$) than pure GMC. While number of apoptotic cells significantly increased with targeted (GMC-CSN-Neu5Ac-NPs, GMC-CSN-Cxmab-NPs, GMC-CSN-Neu5Ac-Cxmab-NPs) CSN-NPs ($p < 0.001$) as compared to pure GMC **(Figure 4.9 B)**. These results supported the efficacy of EGFR and glycan receptor targeting for improving the cytotoxicity in lung cancer cells.

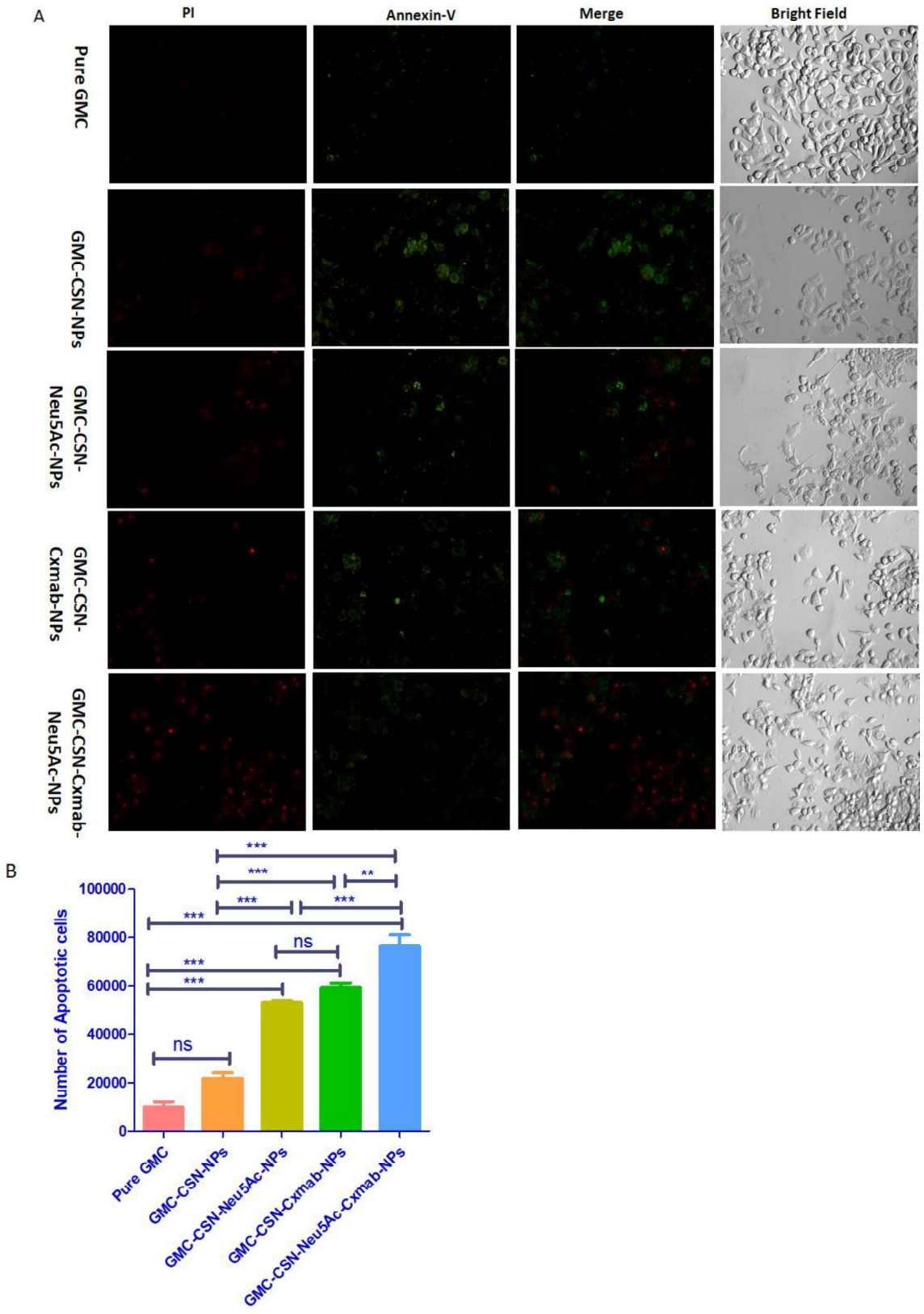

Figure 4.9 A. Confocal laser scanning microscopic analysis for apoptosis by Annexin-V/PI double staining of A-549 cells treated with pure GMC drug, and GMC loaded non-targeted and targeted CSN NPs. Annexin-V staining (green cells) is used to detect early apoptosis

4.5.10 *In vivo* evaluation

4.5.10.1 Pharmacokinetic evaluation of gemcitabine

In vivo pharmacokinetic parameters shown in **Table 4.7** of pure GMC, GMC loaded non-targeted and targeted CSN-NPs were assessed by examination of GMC concentration **(Figure 4.10)**. The pure GMC was instantly excreted from systemic circulation due to short plasma half-life. Although, GMC administered after encapsulating in CSN-NPs was maintained in circulation for extended period of time. The results revealed that pure GMC was not noticeable after 4 h of delivery, while mean residence time (MRT) and half-life ($T_{1/2}$) of GMC were enhanced when encapsulated in targeted CSN-NPs (GMC-CSN-Neu5Ac-Cxmab-NPs > GMC-CSN-Cxmab-NPs > GMC-CSN-Neu5Ac-NPs) than non-targeted CSN-NPs (GMC-CSN-NPs). In particular the total body clearance (CL_T) and elimination rate constant (K_e) of GMC encapsulated in targeted CSN-NPs was lower than non-targeted CSN-NPs and pure GMC, resulting in higher systemic exposure (AUC_{total}) of targeted and non-targeted CSN-NPs leading to higher relative bioavailability (F_R) of CSN-NPs (most with GMC-CSN-Neu5Ac-Cxmab-NPs) as compared to that of pure GMC. It can be suggested that GMC-CSN-Neu5Ac-Cxmab-NPs exhibited extended circulation and higher retention as well as sustained release of GMC due to stealth effect by surface conjugation of CSN with Neu5Ac which inhibits opsonisation.

Table 4.7 Pharmacokinetic parameters of pure GMC, non-targeted and targeted CSN-NPs after *i.v.* administration of GMC

Pharmacokinetic parameters	Pure GMC (Mean ± SD*)	GMC-CSN-NPs (Mean ± SD*)	GMC-CSN-Neu5Ac-NPs (Mean ± SD*)	GMC-CSN-Cxmab-NPs (Mean ± SD*)	GMC-CSN-Neu5Ac-Cxmab-NPs (Mean ± SD*)
AUC_{total} (ng.h/mL)	2519.14±344.43	4086.23±1641.08	4092.92±1378.79	3900.95±230.73	4268.86±1351.87
C_{max} (ng/mL)	2311.65±322.91	1188.903±402.84	1060.77±328.442	1033.79±180.02	944.36±636.63
T_{max} (h)	0.5	0.5	0.5	0.5	0.5
$T_{1/2}$(h)	0.5±0.03	4.89±0.87	4.99±0.79	6.77±2.04	7.86±3.48
MRT(h)	1.16±0.05	5.81±0.03	6.46±0.72	8.44±2.26	10.77±4.69
C_{LT} (L/h)	3.93±0.58	2.68±0.87	2.61±0.75	2.56±0.15	2.51±0.83
Ke (h^{-1})	1.390±0.09	0.144±0.02	0.141±0.02	0.109±0.03	0.100±0.04
V_d (L)	2.83±0.38	19.28±8.13	19.35±8.11	25.07±7.26	28.94±14.46
F_R	-	1.622±0.65	1.624±0.54	1.548±0.09	1.694±053

Note: AUC_{total}: Total Area under the curve, C_{max}: Maximum plasma drug concentration, T_{max}: Maximum Time, $T_{1/2}$: Plasma Half-life, MRT: Mean residence time, V_d: Volume of distribution, C_{LT}: Total body clearance, F_R: Relative bioavailability, Ke: Elimination rate constant. n = 3.

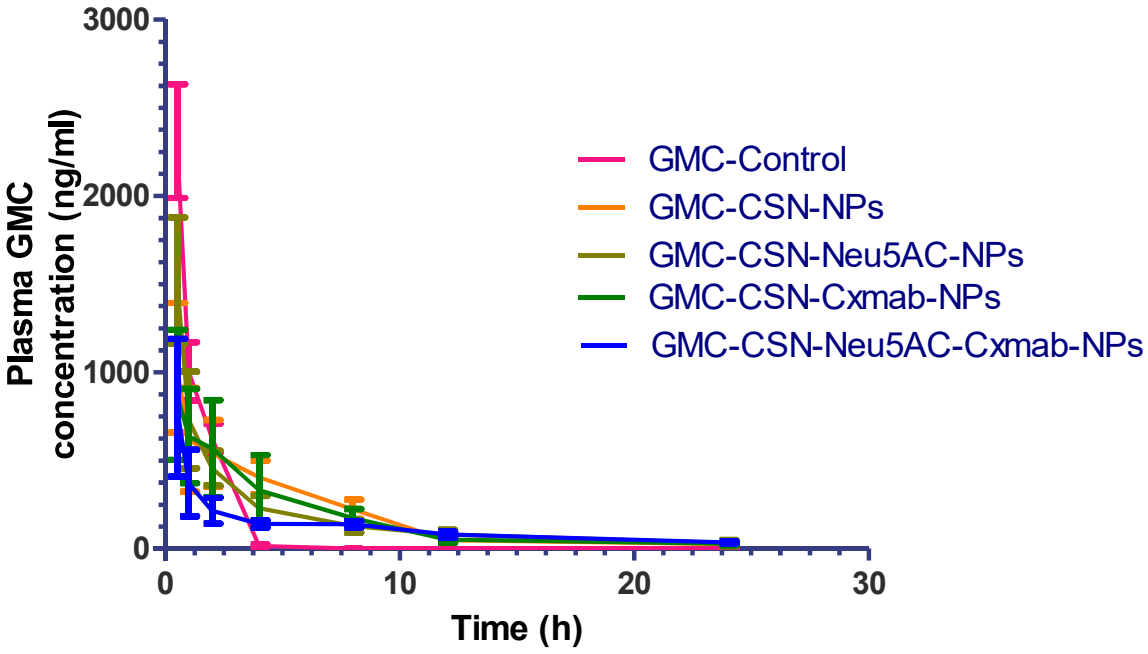

Figure 4.10 *In vivo* Pharmacokinetic study of pure GMC (GMC control) in comparison with non-targeted (GMC-CSN-NPs) and targeted (GMC-CSN-Neu5Ac-NPs, GMC-CSN-Cxmab-NPs, GMC-CSN-Neu5Ac-Cxmab-NPs) CSN-NPs. The data has been presented as mean±SD (n =3).

4.5.10.2 *In-vivo* biochemical estimation

Blood serum biochemistry assay of hepatic [alkaline phosphatase (ALP), alanine aminotransferase (ALT) & aspartate transaminase (AST)] and renal [uric acid, blood urea nitrogen (BUN) & creatinine] toxicities are presented in **Figure 4.11 A & B**. As per the results, the treatment with free GMC leads to significant *(* $p < 0.05$), ($ $p < 0.001$)* elevation in the levels of renal-function related indexes such as uric acid, BUN & creatinine and hepatic-function related indexes including ALP, ALT & AST in the serum as compared to saline control group. Meanwhile, the results revealed that non-significant *(# $p > 0.05$)* variations in the renal & hepatic biomarkers like uric acid, BUN, creatinine, ALP, ALT and AST could be found after the treatment with GMC loaded EGFR and glycan receptor targeted NPs as compared to saline control group. All these results indicate the excellent biocompatibility and minimal toxicity of GMC loaded EGFR and glycan receptor targeted delivery system.

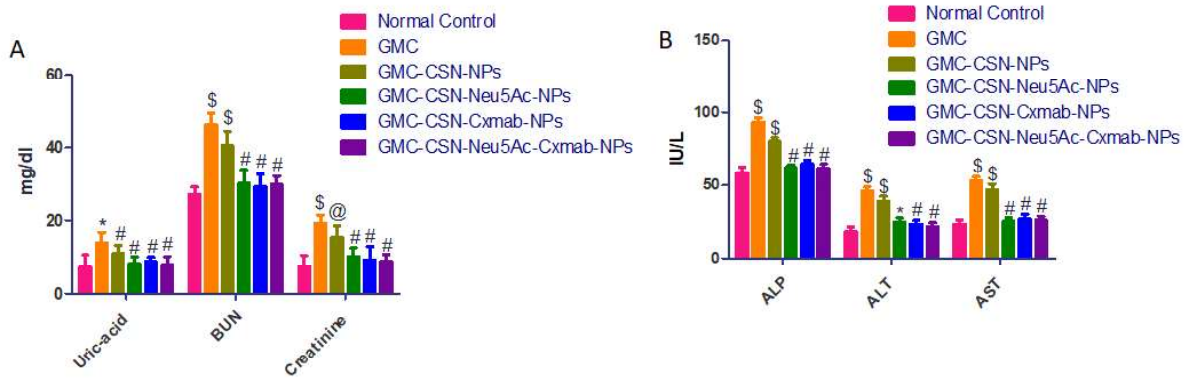

Figure 4.11 Biochemical markers levels for A. kidney function (uric-acid, BUN & Creatinine) and B. liver function (ALP, ALT & AST) in blood serum after the administration of pure GMC, GMC-CSN-NPs, GMC-CSN-Neu5Ac-NPs, GMC-CSN-Cxmab-NPs & GMC-CSN-Neu5Ac-Cxmab-NPs at a dose of 10 mg/kg in comparison with 0.9% saline control. Results are presented as mean ± SD (n=3). The statistical significance between the groups was analysed by t-test *(* $p < 0.05$)*, *(@ $p < 0.01$)* and *($ $p < 0.001$),* respectively, non-significant *(ns) (# $p > 0.05$)* as compared to saline control group.

4.5.10.3 *In vivo* therapeutic efficacy

The H&E stained tissue sections **(Figure 4.12 A)** showed that the lung treated with GMC-CSN-Neu5Ac-Cxmab-NPs had only a few small nodules corresponding to normal negative control (saline treated) group, and most of the lung was free of cancerous lesions in comparison to the animals treated with GMC-CSN-NPs, GMC-CSN-Neu5Ac-NPs, GMC-CSN-Cxmab-NPs. Whereas, metastatic nodules shielded most of the lung when mice were only treated by GMC control alike to positive control (B[a]P treated) group. The results **(Figure 4.12 B)** displayed that GMC-CSN-Neu5Ac-Cxmab-NPs exhibited the strongest anticancer activity due to significant reduction of lung

cancerous cells as compared with positive control group *($p < 0.001$)* and GMC control *($p < 0.05$)*. These results might be explained by the increased local concentration of GMC in the lung cancerous tissue, since higher accumulation of GMC in lung cancerous tissues was favoured by dual receptor targeting and relatively long retention time, which was in good agreement with the results of H&E stained sections of lungs. The therapeutic effect of GMC-CSN-Neu5Ac-Cxmab-NPs was also examined in terms of survival rate of lung cancer bearing mice by Kaplan-Meier survival graph **(Figure 4.12 C)**. All of the mice treated with GMC control died within 8 weeks of treatment, which was might be due to the toxic effects of free GMC. When mice were injected with GMC encapsulated in various targeted and non-targeted CSN-NPs, among all other groups GMC-CSN-Neu5Ac-Cxmab-NPs exhibited a much higher survival rate as all six mice were alive after 16 weeks. The mice group treated with dual receptor targeted group (GMC-CSN-Neu5Ac-Cxmab-NPs) showed an enhanced anticancer efficacy than the targeted, non-targeted CSN-NPs and GMC control treated groups. It was concluded that the cancer targeting ability of GMC-CSN-Neu5Ac-Cxmab-NPs increased survival rates by reducing *in vivo* toxic effects of GMC in normal tissues. As a result, dual receptor targeted nanomedicine can improve the efficacy of anticancer drugs with reduction of dose and the side effects (associated with higher doses).

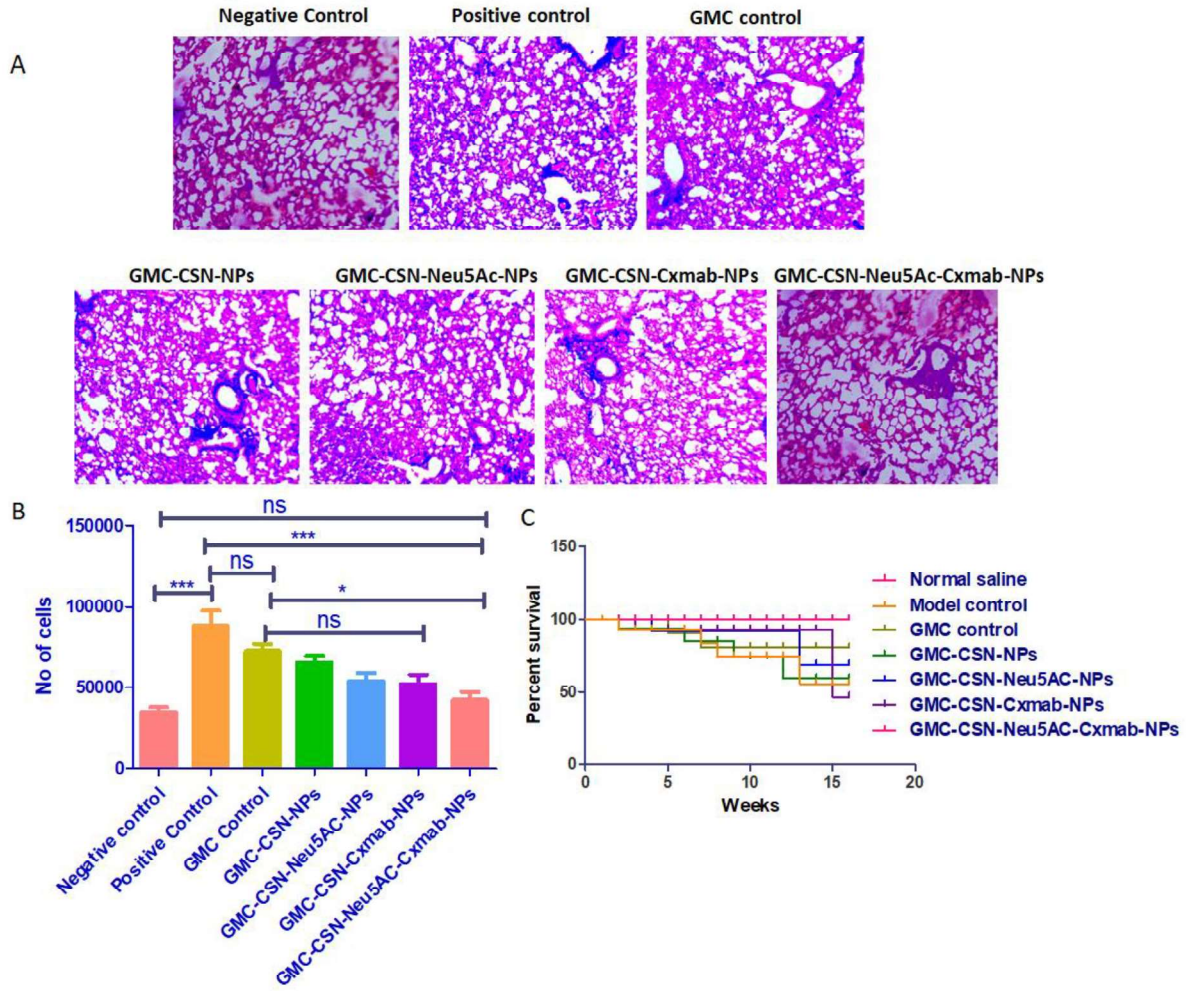

Figure 4.12 A. Histopathological examination of H&E stained lung sections of GMC-CSN-NPs, GMC-CSN-Neu5Ac-NPs, GMC-CSN-Cxmab-NPs and GMC-CSN-Neu5Ac-Cxmab-NPs treated groups in comparison with diseased positive control (B[a]P treated) and normal negative control (saline treated) group. B. Quantification of number of cells in H&E sections of lungs treated with related groups using Image J software, GMC-CSN-Neu5Ac-Cxmab-NPs: $p > 0.05$ vs negative control, *** $p < 0.001$ vs positive control. C. Kaplan–Meier curve comparing mice's survival up to 16 weeks. The Kaplan–Meier curve was plotted using GraphPad Prism 5 to compute survival rate. N (number mice per group) = 6.

4.6 Discussion and Conclusion

In the current study, the chimeric mAb conjugated CSN-NPs loaded with GMC was successfully optimized by the QBD approach. We have developed GMC loaded cetuximab and Neu5Ac conjugated CSN-NPs and demonstrated its therapeutic effects *in vitro* against A-549 lung cancer cells which have overexpressed EGFR and Neu5Ac binding receptors (glycan) and, also *in vivo,* in B[a]P induced lung cancer mice model. These targeting ligands have specific affinity with the cell surface receptors and they can distinguish amongst healthy and cancerous cells, based on the receptors

expression levels [213]. This study indicate that active targeting of dual ligands enhance the therapeutic effects of GMC by enhancing targeting efficiency and reducing nonspecific uptake.

The Neu5Ac conjugation with chitosan (CSN-Neu5Ac) by cabodiimide chemistry was confirmed by ^{1}H NMR, mass and FTIR spectra. These outcomes support the evidence of previously stated study that amine groups (existing at the surface of CSN) covalently conjugate with the carboxylic group (present in folic acid) activated via EDC/NHS to form a amide linkage [274]. Non-targeted and glycan receptor targeted CSN-NPs were formed by ionic gelation technique followed by conjugation of Cxmab through electrostatic interaction. This approach exploits electrostatic interaction between negatively charged Na-TPP and positively charged CSN to formulate uniform NPs dispersion [275].

Particle size is a critical attribute that needs to be carefully monitored because it eventually affects the fate of the nanocarriers (PK & PD) inside the biological system [276]. The particle size of prepared CSN-NPs was less than 200 nm and PDI less than 0.3 supposed to be well monodispersed and ideal for improving drug delivery to cancerous cells. According to published studies that nanoparticles with a size of less than 200 nm are expected to enhance systemic functionality by extending blood circulation, evading the reticuloendothelial system (RES), and enabling passive targeting through enhanced permeation and retention effect (EPR) [277]. Slight increase in particle size of Neu5Ac and Cxmab conjugated CSN-NPs was observed due to the ligand modification on surface CSN with Neu5Ac and substitution of antibody (Cxmab) on the surface of the CSN-NPs. Zeta potential is a significant factor for assessing the stability of NPs in *in vivo* systems [278]. The CSN-NPs have high positive zeta potential that facilitate their uptake in negatively charged cancerous cells [279]. Zeta potential of CSN-NPs decreased from 52.83±1.90 to 28.73±3.72 mV, which may be explained by the negative charge associated with Neu5Ac and Cxmab that interact through electrostatic interaction with cationic charge of CSN on the surface. The reduction in zeta potential further suggest that Neu5Ac and Cxmab were tightly conjugated on the surface of CSN-NPs. The % EE of CSN-NPs was above 60%, indicating efficient entrapment ability of the drug in CSN-NPs. The entrapment efficiency of Neu5Ac and Cxmab targeted CSN-NPs was lower (62.86±1.60) than non-targeted CSN-NPs (69.33±2.49) due to stearic hindrance of Neu5Ac and Cxmab on the surface of dual receptor targeted

CSN-NPs. The morphology of prepared CSN-NPs were verified by SEM, TEM, SAD and AFM analysis that indicated formation of uniform spherical smooth surface particles with narrow size distribution which nay also correlated with particle size measurement from dynamic light scattering analysis from Zetasizer.

The conjugation of targeting ligands (cetuximab and Neu5Ac) was also confirmed by XPS analysis. Differential elemental composition of nitrogen, oxygen, and carbon on the surface of NPs indicated by XPS analysis suggested that Cxmab and Neu5Ac were conjugated on the surface of GMC-CSN-NPs. The rise in the proportion of N1s and C1s in GMC-CSN-Neu5Ac-NPs can be attributed to the presence of Neu5Ac on the surface of NPs. The proportion of nitrogen in GMC-CSN-Cxmab-NPs (13.6%) and GMC-CSN-Neu5Ac-Cxmab-NPs (11.5%) increases due to coating of Cxmab on GMC-CSN-NPs (6.29%) and GMC-CSN-Neu5Ac-NPs (6.6%) respectively**.** This is due to the high proportion of nitrogen atoms in Cxmab. Our findings are also in line with a previous study which demonstrated that the existence of herceptin on docetaxal loaded NPs surface as confirmed by XPS [280].

The status of encapsulated drug in the nanoparticles is very essential for the drug delivery mechanism. So the physical state of GMC in CSN-NPs was evaluated in comparison with free GMC using XRD, DSC and FTIR. The XRD spectra of GMC exhibited crystalline character due to the presence of abundant peaks, while these peaks were missing in the spectrum of targeted and non-targeted CSN-NPs. The DSC thermogram of the free GMC revealed crystalline structure that was indicated by a strong melting peak. Conversely, GMC present in CSN-NPs, showed no peak at its melting point showing that GMC was incorporated in CSN-NPs in an amorphous state. In the FTIR analysis the major peaks of gemcitabine disappeared and shifted in targeted and non-targeted CSN-NPs. This indeed validated the fact that GMC was entrapped into the polymeric matrix of CSN-NPs. The presence of drug in nanocarrier was confirmed by XRD, DSC and FTIR in accordance with previous reports and the results suggest that doxorubicin was successfully loaded in nanoparticles [281].

The amount of conjugation or ligand density influences the therapeutic effectiveness of targeted nanoparticles. Targeted nanotherapeutics always elicit greater biological response, greater the degree of conjugation higher will be the therapeutic response up to a particular limit [282]. Bradford assay was used to analyse the extent of cetuximab conjugation on CSN-NPs and was found to be 72.94 ± 3.47% in GMC-CSN-Cxmab-NPs and 63.20 ± 2.12% Cxmab in GMC-CSN-Neu5Ac-Cxmab-NPs. The analysis was performed base on previously reported study on conjugation of mAb cetuximab on the surface of docetaxel loaded PLGA NPs surface and was determined by the Bradford assay [248]. The Neu5Ac content was quantified to be 78.50 ±3.32%, 67.22 ± 2.36% and 58.46 ± 2.20% in CSN-Neu5Ac conjugate, GMC-CSN-Neu5Ac-NPs and GMC-CSN-Neu5Ac-Cxmab-NPs respectively.

The release of drug from nanoformulations plays an important role to examine the *in vivo* performance. The prepared CSN-NPs showed a pH-dependent controlled release of GMC. Sustained release of drug was observed at physiological condition (pH 7.4) with burst release in the tumor microenvironment (pH 5.5). Thus, CSN was ionised at lower pH due to the protonation of its amino groups, allowing GMC to move out rapidly from CSN-NPs. Our findings coincide with the results of gemcitabine encapsulated silk fibroin nanoformulation for lung cancer treatment, where drug release was higher at pH 5 than 7.4 [218]. Enhanced release of drugs in cancerous cells in comparison to healthy cells and tissues could raise therapeutic effectiveness and diminish undesirable effects [16]. Furthermore, release patterns showed substantial pH dependency, ensuring chitosan nanoparticles as ideal candidate for cancer specific drug delivery [283]. We anticipate that GMC release from CSN-NPs in the cancerous region to have the desired therapeutic impact.

Utilizing *in vitro* A549 cell line model, the therapeutic effect of CSN-NPs was compared with unbound GMC by means of MTT assay for cell viability. GMC-loaded CSN-NPs had considerably greater dose-related cell cytotoxicity than free GMC. *In vitro* MTT assay demonstrated enhanced cellular killing by GMC-CSN-Neu5Ac-Cxmab-NPs due to the selective uptake by EGFR and glycan receptors in A-549 lung cancer cells suggesting the efficacy of targeted molecular therapeutics. This may be due to rapid efflux of free drug out of the cell by P-glycoprotein [284], but the dual receptor

targeted CSN-NPs could traffic the bound drug into cancerous cells and slowly release the drug within target cells due to target cell specificity. Cellular uptake of GMC-CSN-Neu5Ac-Cxmab-NPs revealed higher uptake in A-549 cells. This could be linked to the interaction between the negative charge on highly expressed phospholipids in cancerous cells and the cationic surface charge on the coated CSN-NPs, which results in enhanced cancer site deposition and cytotoxicity [261]. Specific uptake relies on receptor-triggered endocytosis of the drug nanocarrier. Both EGFR and glycan receptor targeting ligands were taken up by ligand-induced receptor mediated internalization [154]. The results of uptake and cytotoxicity experiments indicate that GMC-CSN-Neu5Ac-Cxmab-NPs can be employed as promising nanocarriers to facilitate the therapy of NSCLC, illustrating increased therapeutic activity at lower doses.

NSCLC is a challenging and heterogeneous illness that has been detected to spread in the surrounding organs due to its metastatic tendency. The emergence of metastases decreases the efficacy of therapy, resulting in higher fatality rates. The potential of developed dual receptor CSN-NPs to suppress the metastatic activity of NSCLC was next studied by utilising a wound healing assay [261]. The wound healing assay results showed that GMC-CSN-Neu5Ac-Cxmab-NPs suppress metastasis more effectively than other CSN-NPs. Annexin-v/PI apoptosis assay in A-549 cells showed significantly higher apoptosis upon treatment with GMC-CSN-Neu5Ac-Cxmab-NPs as compared to other CSN-NPs. A previous study showed that as compared to the non-targeted NPs, molecular targeted NPs showed greater level of cell apoptosis [6].

We anticipate that the developed nanoparticles (dual receptor targeting pH responsive CSN-NPs) might be more effective, not merely because of their EPR effect and that of release the drug in the cancer tissue proximity due to lowered pH environment, but additionally due to dual receptor selective drug delivery potential of Neu5Ac and Cxmab-modified CSN-NPs. As a result, particles can gather in the target tissues, result in reduction of the required therapeutic dose as well as undesirable toxic effects of drug.

As described previously, after intravenous injection, GMC is metabolised by the cytidine deaminase enzyme, which is mostly found in blood, healthy tissue, and cancerous tissues [252]. Dual receptor-targeted CSN-NPs improve specificity and inhibit metabolization, resulting in increased therapeutic effects of GMC at the desired site. A variation in the pharmacokinetic data is indicative of the extended residence time in circulation. Further, *in vivo* pharmacokinetic findings confirm the prolonged-circulating behaviour of the prepared nanoformulations. The t1/2 and MRT of GMC in CSN-NPs was enhanced, whereas systemic exposure (AUC_{total}) was noticeably increased with a simultaneous decrease in drug clearance as compared to pure GMC. Similar, results have been reported for paclitaxel loaded targeted nanoemulsion which showed prolonged mean residence time (MRT) and elimination half-life ($T_{1/2}$) in Sprague Dawley rats [285]. The dual receptor targeted NPs (GMC-CSN-Neu5Ac-Cxmab-NPs) exhibited higher anticancer activity due to significant reduction of lung cancerous cells compared to GMC control ($p < 0.05$) treated group and increased survival rates and lessened mortality by reducing *in vivo* toxic effects of GMC in normal tissues. This indicates that targeting both EGFR and glycan receptors on the same NPs exhibited superior selectivity to lung cancer cells that overexpressed both these receptor in comparison to CSN-NPs targeted with single targeting ligand.

In conclusion the GMC-CSN-Neu5Ac-Cxmab-NPs achieved synergistic cancer cell targeting ability and low systemic toxicity. The dual-receptor targeted CSN-NPs significantly improved specificity while simultaneously enhancing cellular uptake, presenting an opportunity to enhance active targeting of cancerous cells over traditional, single-receptor targeted approaches. These results support the potential application of EGFR and glycan receptor targeted CSN-NPs for encapsulation of GMC for improving cellular internalization, cytotoxicity, and apoptosis with better bioavailability and *in vivo* therapeutic efficacy in NSCLC treatment. The end product could serve as an effective targeted nanotherapeutics for lung cancer treatment.